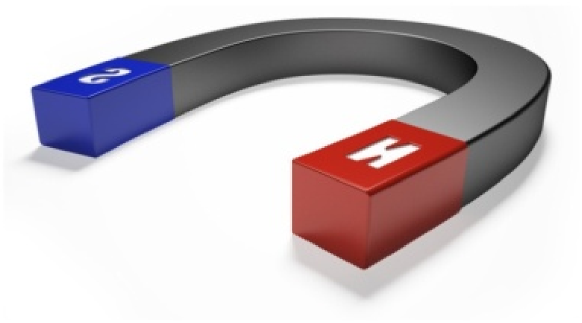

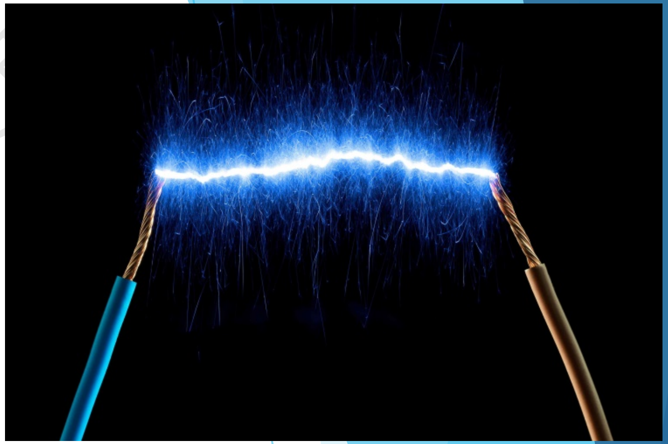

Spin-Orbit Interaction in Magnetic Semiconductors

磁性半导体中自旋轨道相互作用

Xinyu Liu

刘新宇

Department of Physics, University of Notre Dame

半导体学报

IOP Journal of Semiconductors

半语-益言 June 2, 2021

Pre-History

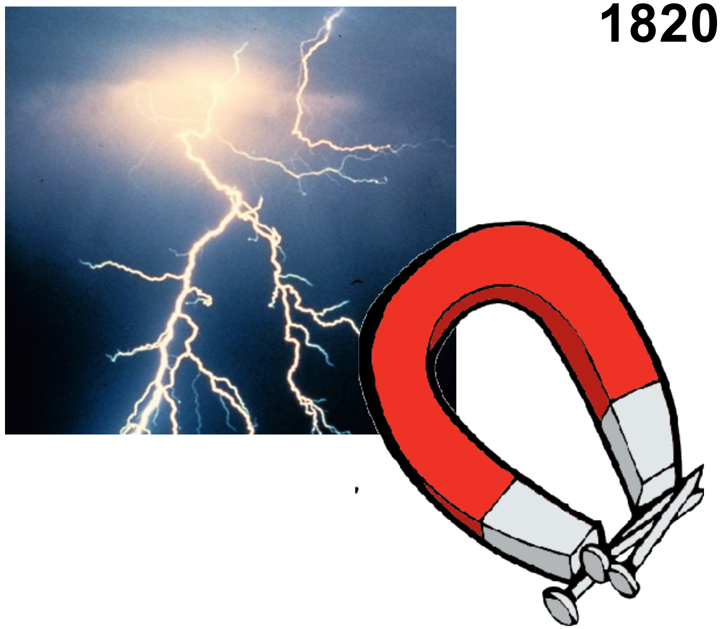

1820: Electric current generates magnetic field

Hans Christian Ørsted

The electron spin degree of freedom

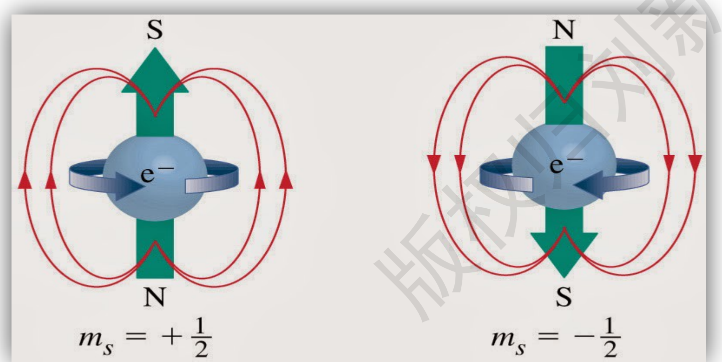

$$\left(\mathbf{i}\hbar\gamma^{\mu}\nabla_{\mu} - \mathbf{mc}\right)\psi = 0$$

Dirac, Paul A.M. (1 February 1928). "The Quantum Theory of the Electron". Proceedings of the Royal Society of London A. 117 (778): 610–24.

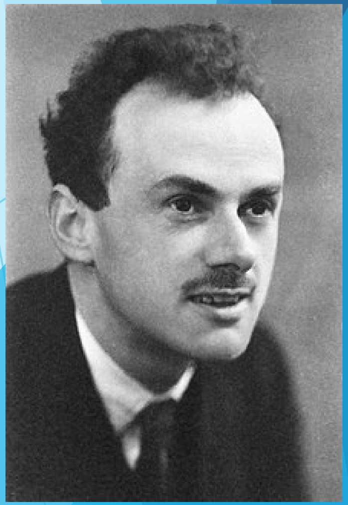

電流產生的磁場/ 自旋磁矩

Spintronics Timeline

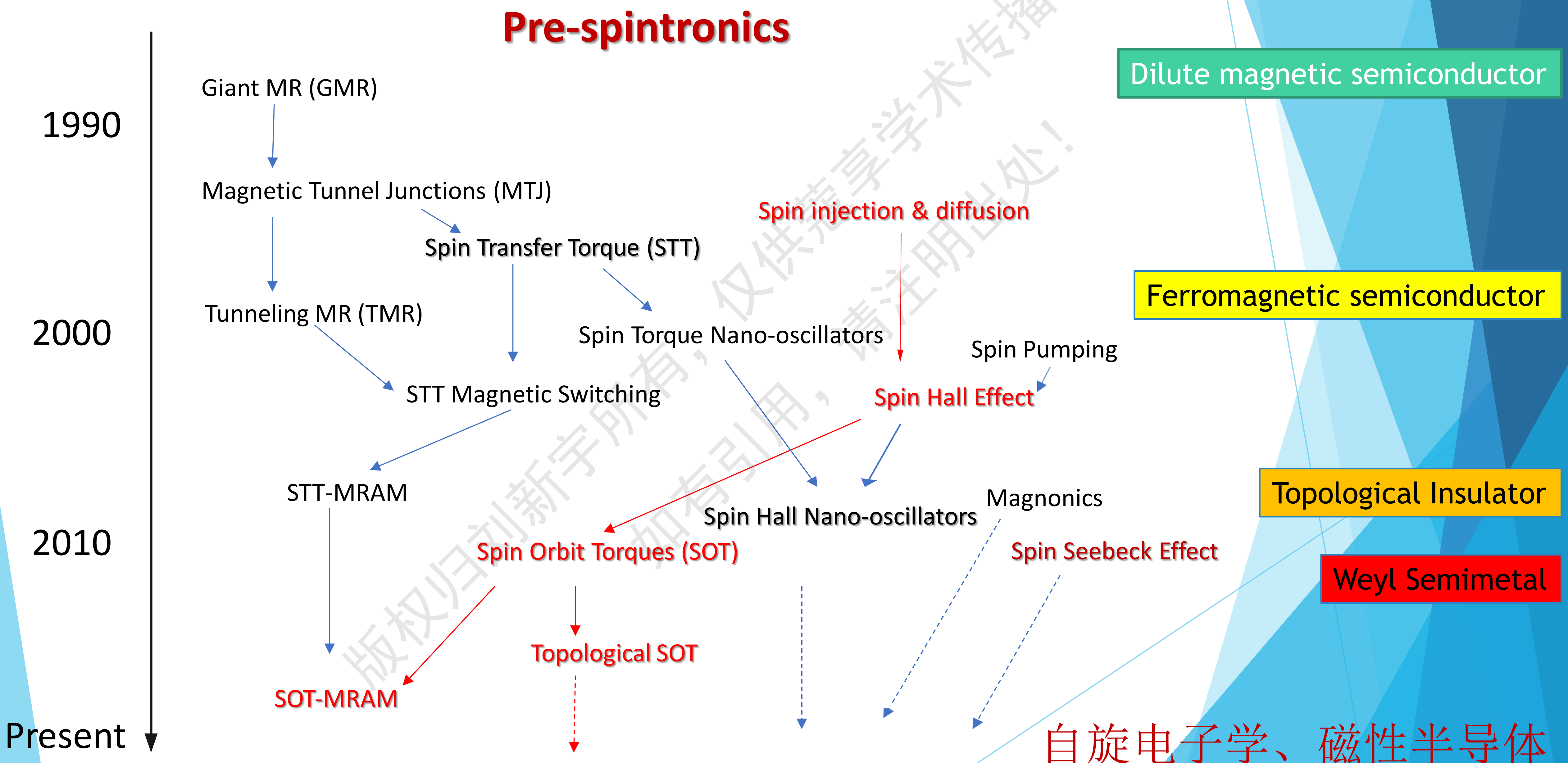

自旋电子学、磁性半导体

Giant magnetoresistance (GMR) multilayers: the dawn of spintronics

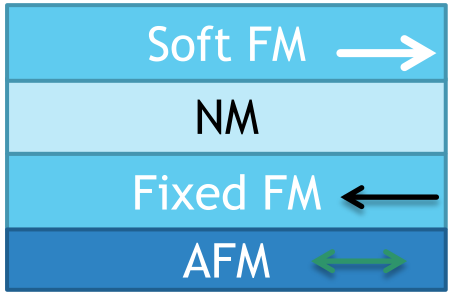

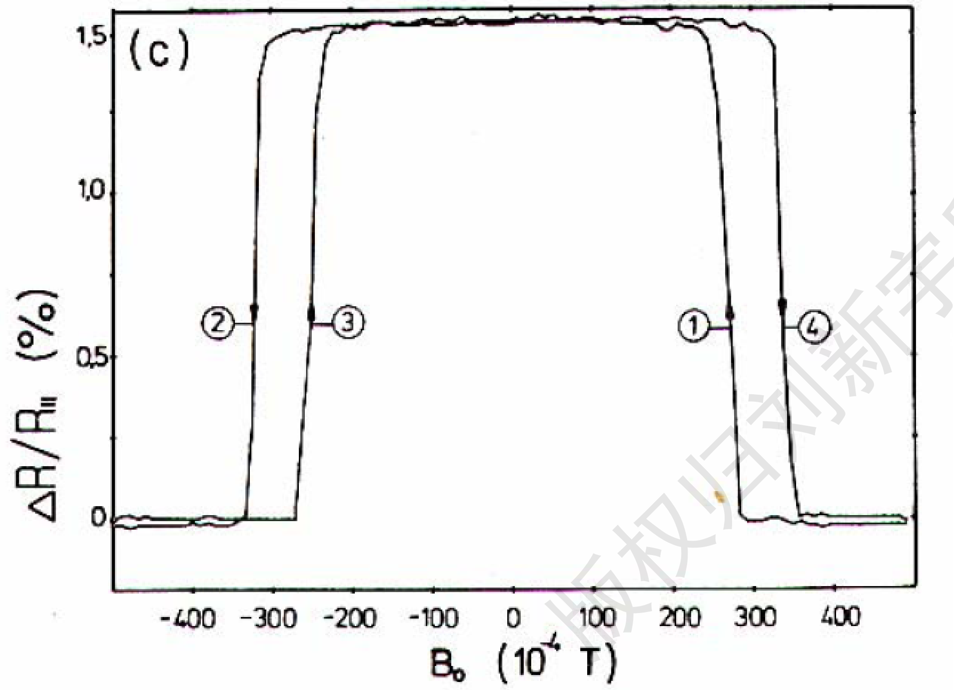

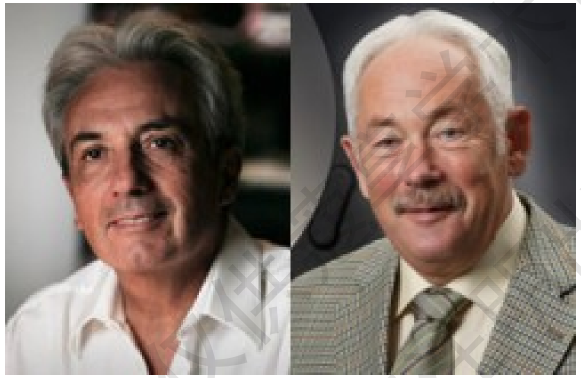

Fert, Grünberg, et al. 1988
Nobel Prize 2007

State of the art

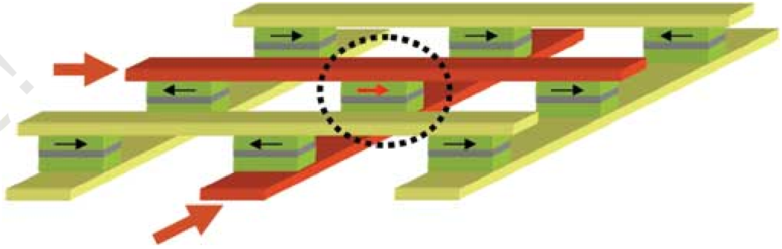

异向磁阻，巨磁阻，隧穿磁阻效应

Brief History of Magnetic Semiconductors

$II_{1-x}Mn_xVI$ semimagnetic semiconductors

- Plasma effects in $II_{1-x}Mn_xVI$ alloys – helicon waves
- Consequences of sp-d exchange interaction
  - Electrical transport studies
  - Optical studies
  - Unique opportunities in 2-D systems
  - Spin entanglement
- Magnetic properties
  - Discovery of spin-glass phase
  - Neutron scattering

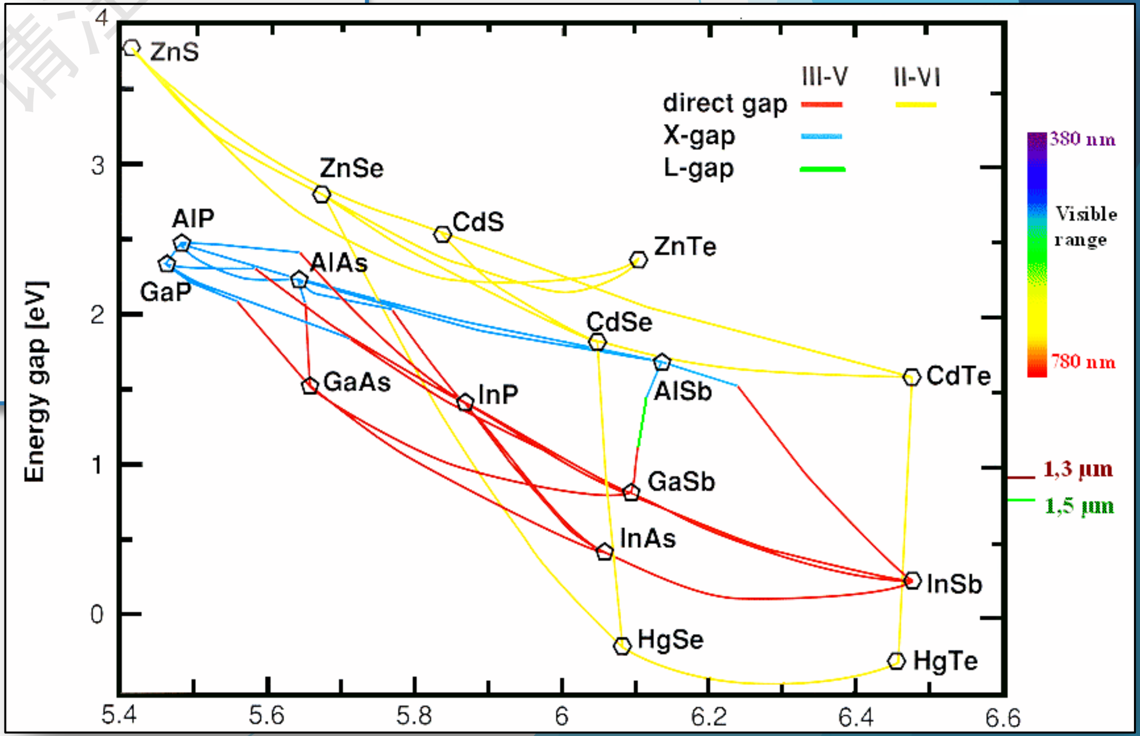

二六族磁性半导体

Pioneer work: $Hg_{1-x}Mn_xTe$

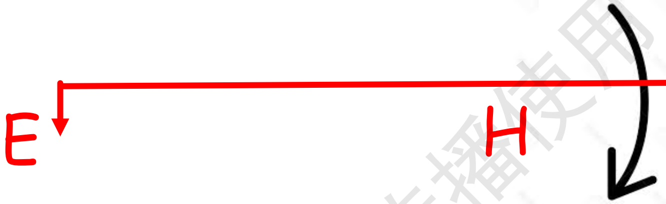

- Helicon-excited EPR in $Hg_{1-k}Mn_kTe$
- Motivation:
  - Enormous enhancement of H
  - Negative ϵ and μ
    - $\omega_c = eB/m^* \gg \omega, 1/\tau$;
    - $(\omega_p)^2 = ne^2/(m^*\epsilon) \gg \omega\omega_c$

$$E/H = [(\mu_o \omega B)^{1/2}]/ne$$

$$e^{-\beta x}$$

$$\beta = \beta_o + \tfrac{1}{2}(\mu_o \omega n e/B)\chi''$$

R. T. Holm and J. K. Furdyna, Observation of helicon-excited electron paramagnetic resonance in $Hg_{1-x}Mn_xTe$, Solid State Commun. **15**, 1459 (1974).

D. P. Mullin, R. R. Gałązka, and J. K. Furdyna, Microwave helicon propagation and the dynamic magnetic susceptibility in $Hg_{1-x}Mn_xSe$, Phys. Rev. B 24, 355 (1981).

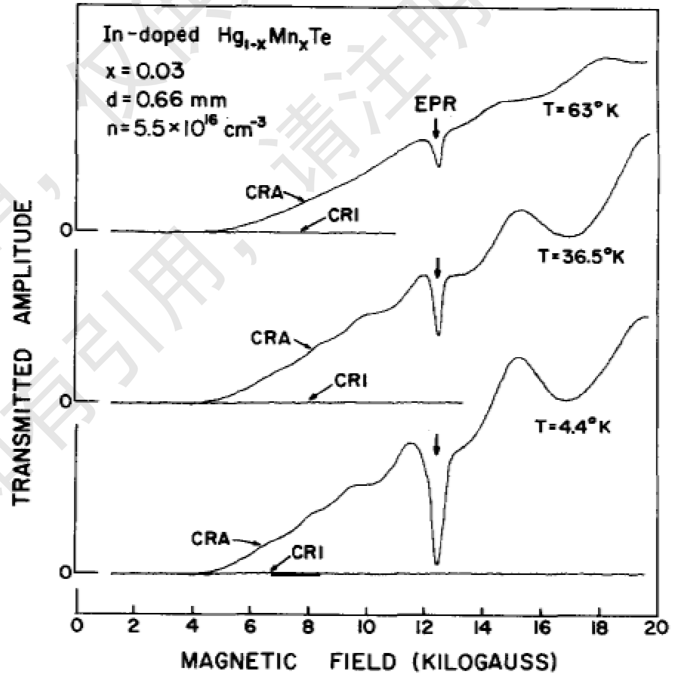

FIG. 3. Transmitted helicon (CRA) amplitude in In-doped crystal ($n = 5.5 \times 10^{16}$ cm^{-3}) as a function of B at 4.4, 36.5 and 63 K. No transmission is observed for the CRI polarization.

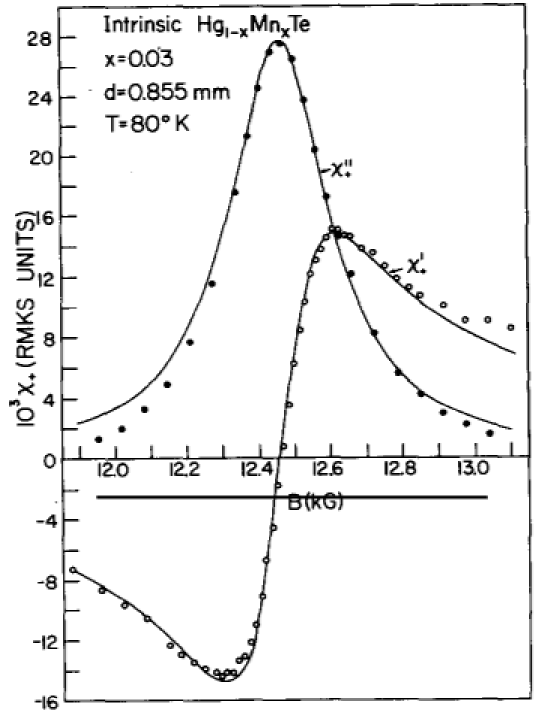

FIG. 2. Real and imaginary parts of the dynamic susceptibility χ_+ as a function of B, corresponding to the data of Fig. 1 in the immediate vicinity of EPR.

电子顺磁共振

Effects of Mn on energy band structure: The *sp-d* Exchange Hamiltonian

SMSC

$$H_T = H_0 + H_{ex}$$
$$= H_0 + \Sigma_i J^{sp\text{-}d}(r - R_i)S_i \cdot \sigma$$

J. Kossut, pss (b) 72, 359 (1975)

This leads to an enormously large g-facto
e.g., for electronic states

$$g_{eff} = g^* + \alpha \underline{\mathbf{M}}/(2\mu_B{}^2H) \text{ [ELECTRONS]}$$
$$g_{eff} = g^* + \beta \underline{\mathbf{M}}/(2\mu_B{}^2H) \text{ [HOLES]}$$

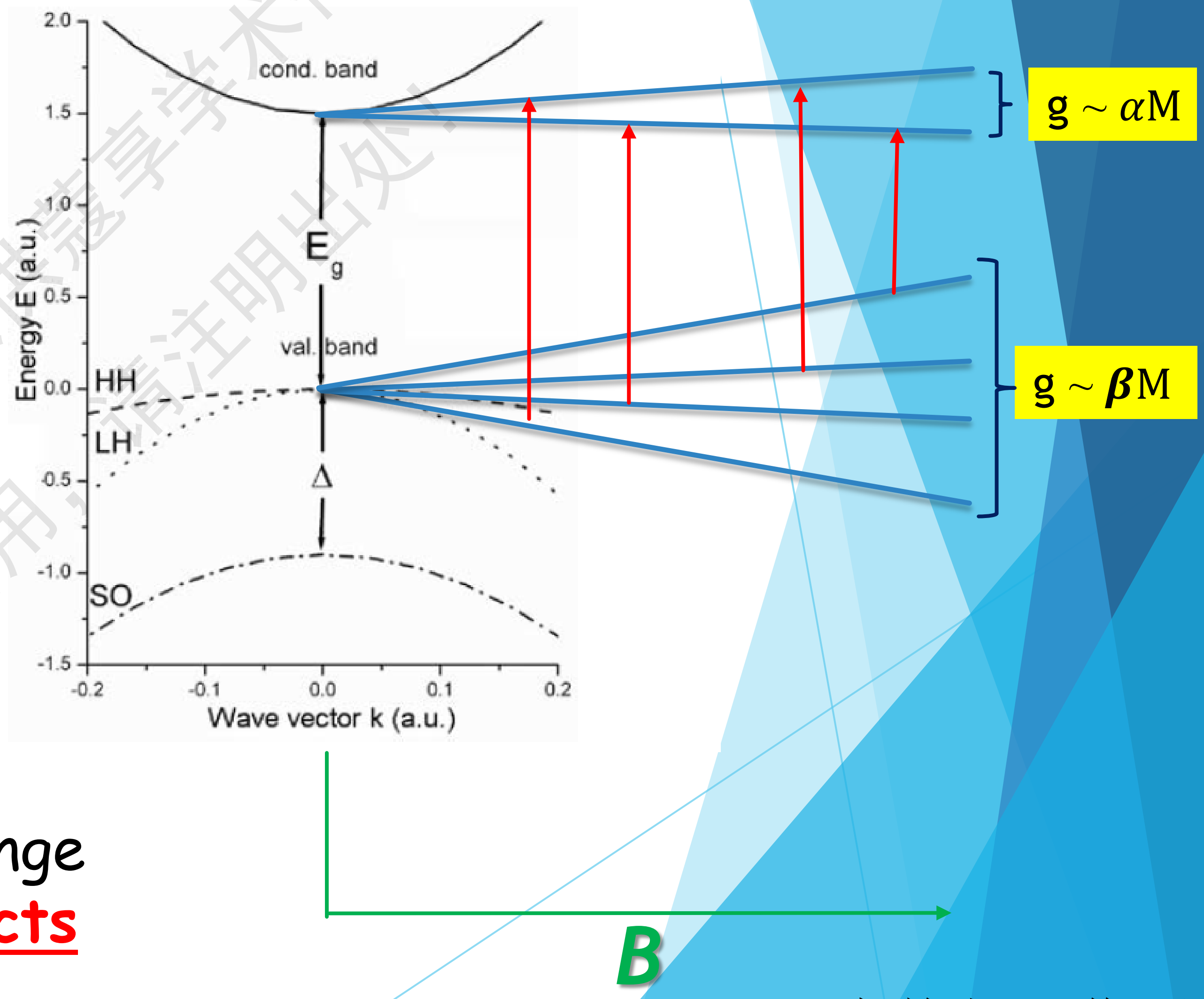

Note: g_{eff} ~ M [**M** gives rise to an exchange field, which is like a magnetic field, **but acts only on spins**]

sp-d 交换相互作用

Consequences of sp-d exchange interaction

- Giant Zeeman splitting of electron states and energy bands and
  - Giant splitting of Landau levels
  - Giant Faraday rotation
  - Optical isolators
- Formation of magnetic polarons
- Insulator – metal transition
- Observation of spin entanglement
- Paved the way to the field of spintronics

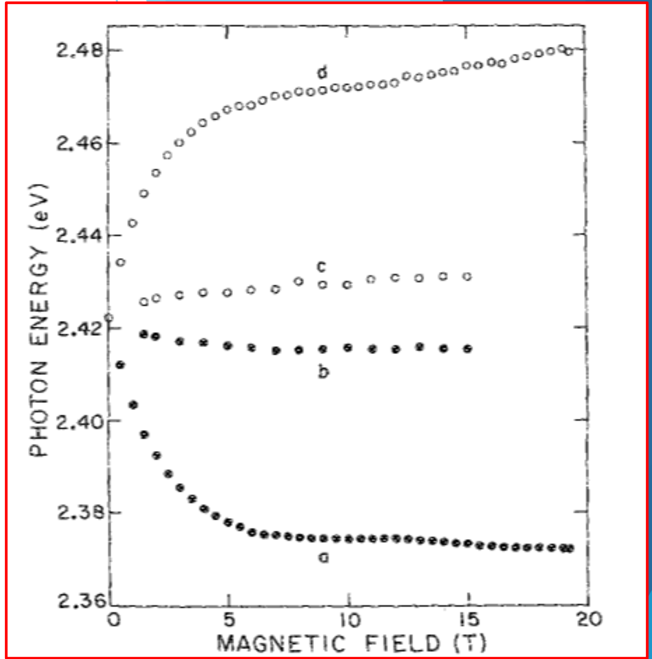

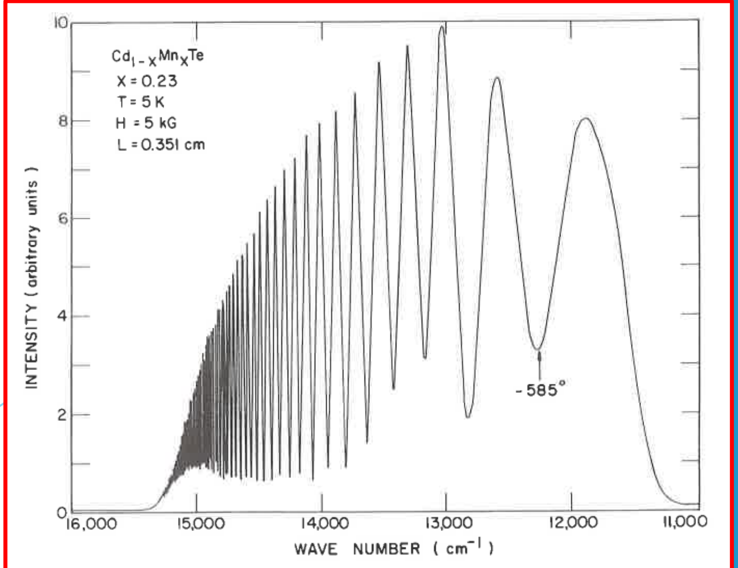

巨塞曼分裂

Ferromagnetic Semiconductor

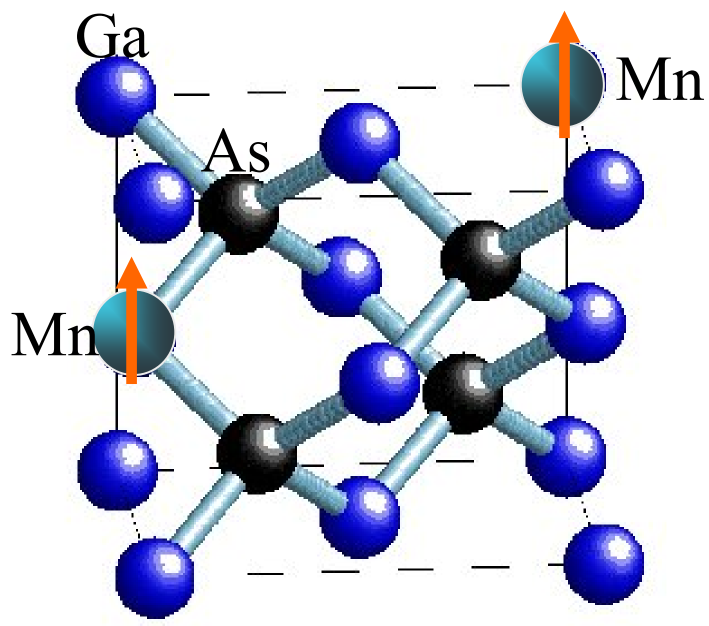

GaAs -
standard III-V semiconductor

Group-II Mn -
dilute magnetic moments & holes

(Ga,Mn)As - ferromagnetic semiconductor

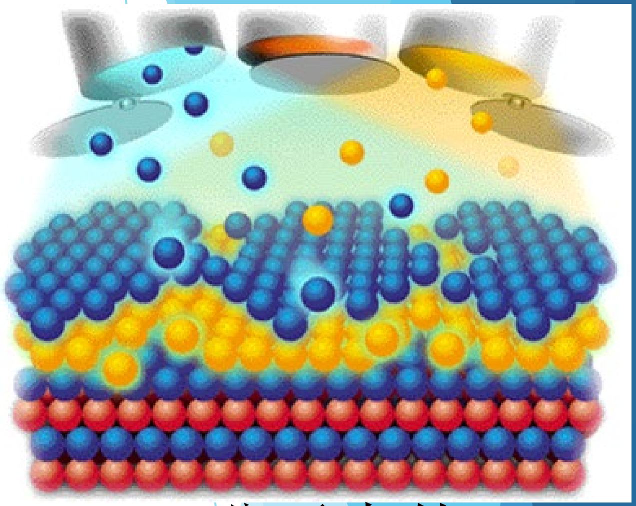

MBE分子束外延

- carriers with both strong SO coupling and exchange splitting, yet simple semiconductor-like bands

- Mn $3d^5$ (S=5/2, L=0): no SO coupling just help to stabilize ferromagnetism

- AHE, GMR, AMR (GPHE), TAMR, Coulomb blockade AMR etc.

Favorable systems for exploring physical origins of old spintronics effects and for finding new ones

三五族铁磁半导体

Beyond III-Mn-V ferromagnetic semiconductor

III = I + II → Ga = Li + Zn

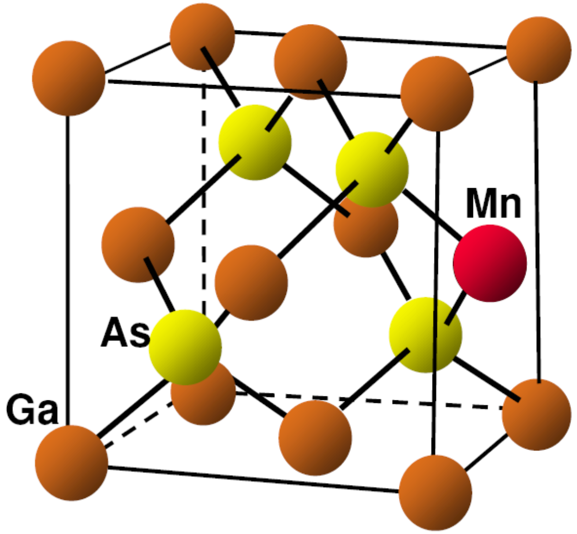

GaAs and LiZnAs are twin SC

(Ga,Mn)As and Li(Zn,Mn)As

should be twin ferromagnetic SC

But Mn isovalent in Li(Zn,Mn)As

→ no Mn concentration limit

→ possibly both p-type and n-type ferromagnetic SC

(Li / Zn stoichiometry)

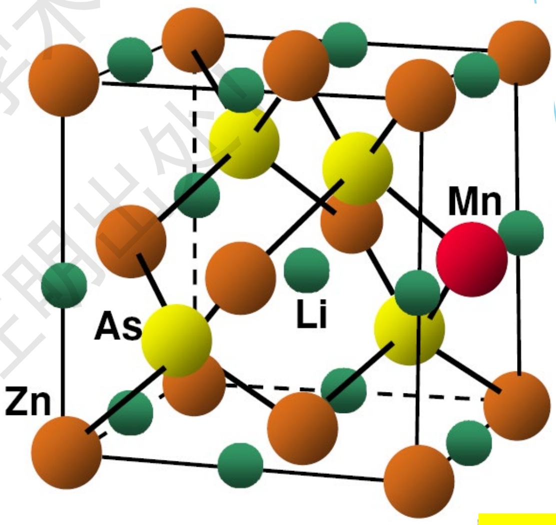

Masek et al. PRL 07

Fe instead of Mn, GaFeSb etc.;
Other magnetic elements: Cr, Gd, Eu …;
Other semiconductor hosts;
………
From Ferromagnet to Antiferromagnet, magnetic topological insulator

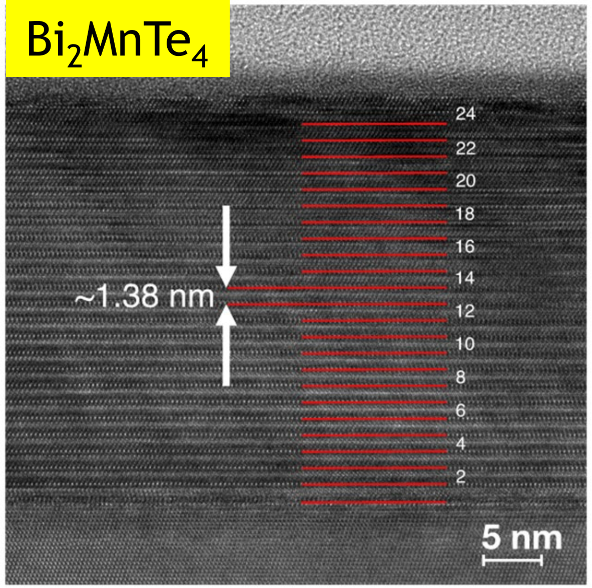

Origin of spin-orbit (SO) interaction

Spin-orbit interation $\mathbf{E} = -\mu_B \mathbf{B}_{eff}$ due to orbital motion

magnetic moment of electron

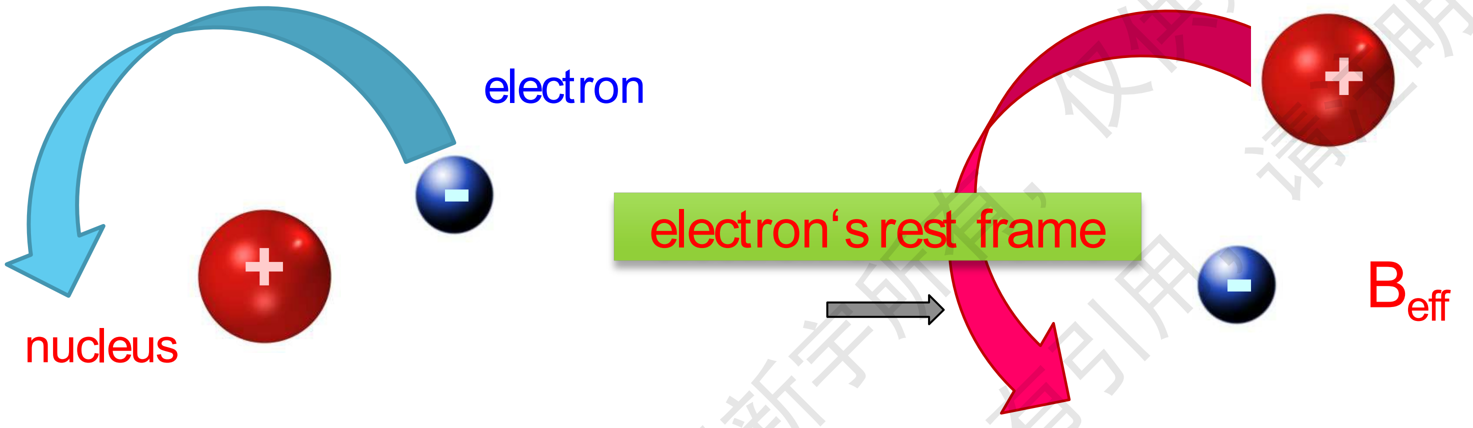

$$\hat{H}_{SO} = -\mu_B \hat{\boldsymbol{\sigma}} \cdot \left[\frac{\mathbf{E} \times \mathbf{p}}{2mc^2} \right]$$

vector of Pauli spin matrices

$$\mathbf{B}_{eff} = \frac{\mathbf{E} \times \mathbf{p}}{2mc^2}$$

$$\hat{H}_{Zeeman} = -\mu_B \hat{\boldsymbol{\sigma}} \cdot \mathbf{B}$$

Spin-orbit coupling term couples spin of the electron $\boldsymbol{\sigma}=2\mathbf{S}/\hbar$ with movement of the electron $m\mathbf{v} = \mathbf{p} - e\mathbf{A}$ in presence of electrical field **E.**

$$H_{SOC} = -\frac{e\hbar}{4m^2c^2} \boldsymbol{\sigma} \cdot [\mathbf{E} \times (\mathbf{p} - e\mathbf{A})]$$

The maximal coupling is obtained when all three componets are perpendicular each other.

The spin-orbit term can be determined from solution of electron state in relativistic case. The equation describing relativistic electron is called Dirac equation, relativistic analogue of Schrodinger equation.

自旋轨道相互作用

Dirac equation: non-relativistic limit

$$i\hbar\frac{\partial\psi(\mathbf{r},t)}{\partial t} = \hat{H}\psi(\mathbf{r},t) = (c\tilde{\alpha}\cdot\hat{\mathbf{p}} + \tilde{\beta}mc^2)\psi(\mathbf{r},t)$$

When Dirac equation is solved up to order $1/c^2$, we get

$$\hat{H} = \frac{1}{2m}\left(\frac{\hbar}{i}\nabla - e\mathbf{A}(\mathbf{r})\right)^2 + V(\mathbf{r}) + mc^2 \quad \text{Unrelativistic Hamiltonian}$$
$$- \frac{e\hbar}{2m}\boldsymbol{\sigma}\cdot\mathbf{B} \quad \text{Zeeman term}$$
$$- \frac{e\hbar}{4m^2c^2}\boldsymbol{\sigma}\cdot[\mathbf{E}\times(\mathbf{p}-e\mathbf{A})] \quad \text{Spin}-\text{orbit coupling}$$
$$- \frac{1}{8m^3c^2}(\mathbf{p}-e\mathbf{A})^4 \quad \text{Mass of electron increases with speed}$$
$$+ \frac{\hbar^2 e}{8m^2c^2}\nabla^2 V(\mathbf{r}) \quad \text{Darwin term}$$

$$-\frac{e\hbar}{4m^2c^2}\boldsymbol{\sigma}\cdot[\mathbf{E}\times(\mathbf{p}-e\mathbf{A})]$$
$$= -\frac{e\hbar}{4m^2c^2}\boldsymbol{\sigma}\cdot[\mathbf{E}\times\mathbf{p}] + \frac{e^2\hbar}{4m^2c^2}\boldsymbol{\sigma}\cdot[\mathbf{E}\times\mathbf{A}]$$
$$= H_{SOC} + H_{AME}$$

AME=Angular magneto-electri

Darwin term: electron is not a point particle, but spread in volume of size of Compton length $\approx \hbar/mc$.

狄拉克公式

Electric field *E* in solids (semiconductor)

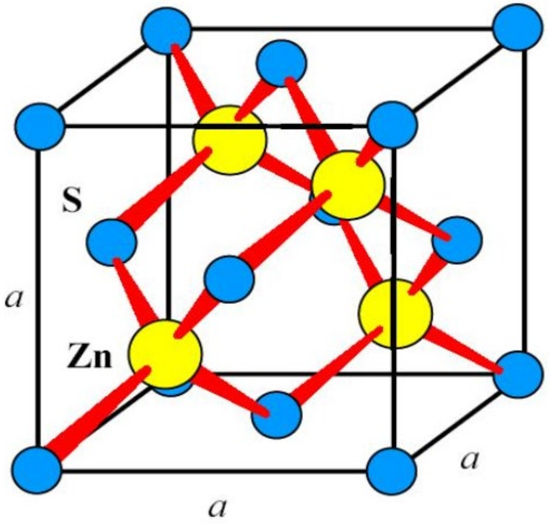

Bulk inversion asymmetry (BIA)
Lack of inversion symmetry in III-V semiconductors
"Dresselhaus contribution γ"

$$B_{BIA} \propto \gamma \begin{pmatrix} k_x \\ -k_y \end{pmatrix}$$

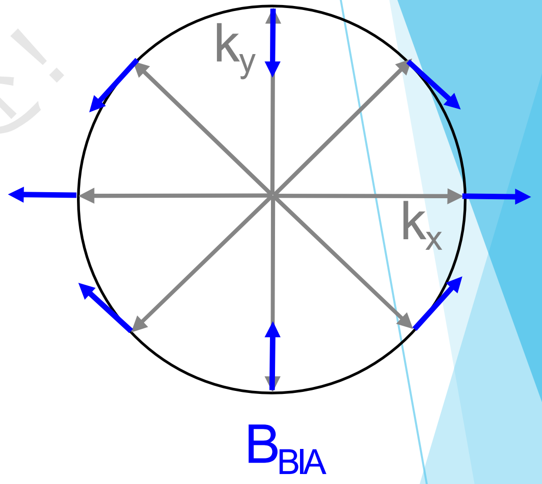

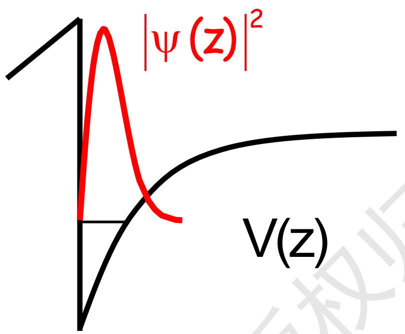

Structure inversion asymmetry (SIA)
due to macroscopic confining potential:
"Rashba contribution α". Tunable by external electric field!

$$B_{SIA} \propto \alpha \begin{pmatrix} k_y \\ -k_x \end{pmatrix}$$

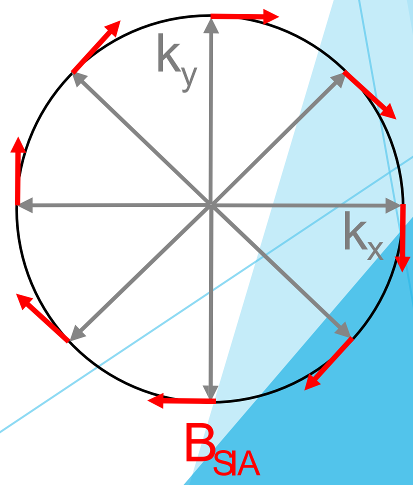

中心反演不对称性

SO interaction in 2DEG: Rashba & Dresselhaus terms

$$\mathbf{H} = \frac{\hbar^2 k^2}{2m} + \mathbf{H}_{SO} \quad \text{with}$$

tunable by gate voltage

Pauli spin matrix

$$\mathbf{H}_{SO} = \alpha(\boldsymbol{\sigma}_x k_y - \boldsymbol{\sigma}_y k_x) + \gamma(\boldsymbol{\sigma}_x k_x - \boldsymbol{\sigma}_y k_y)$$

Rashba — Dresselhaus

(a) $E^{\pm}(\boldsymbol{k}) = \dfrac{\hbar^2 \boldsymbol{k}^2}{2m^*}$

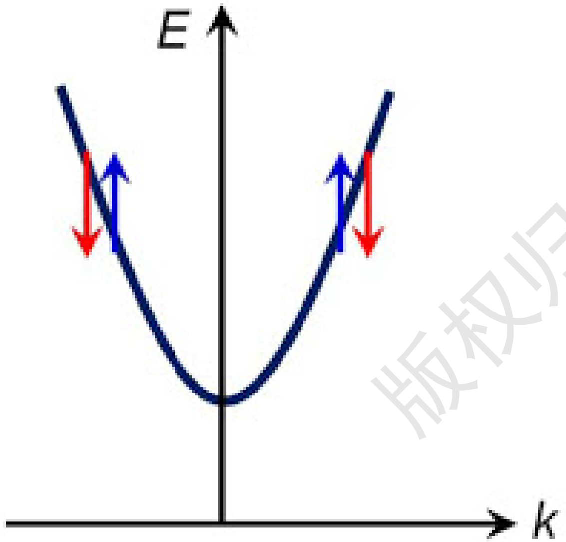

(b) $E^{\pm}(\boldsymbol{k}) = \dfrac{\hbar^2 \boldsymbol{k}^2}{2m^*} \pm \alpha_R |\boldsymbol{k}|$

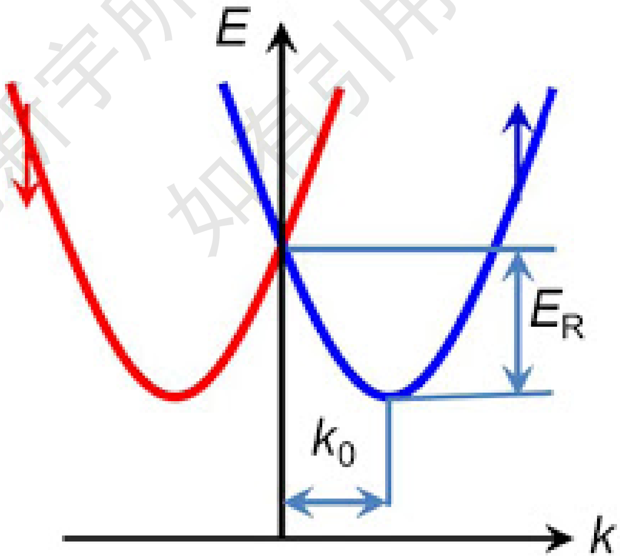

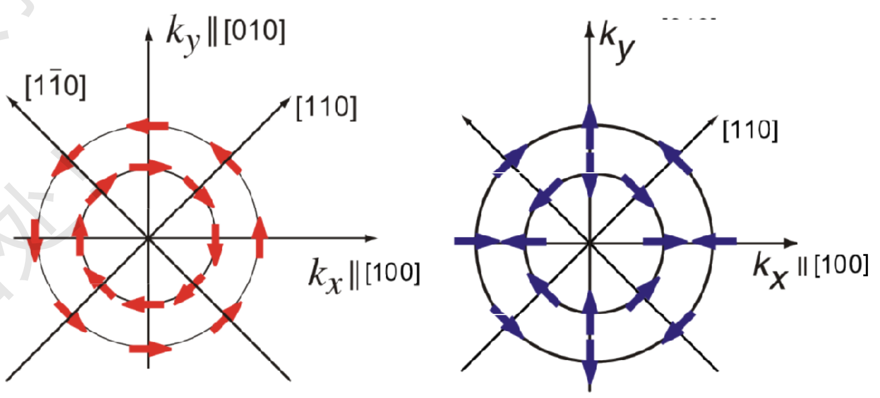

BIA=0
SIA≠0

BIA≠0
SIA=0

$$E = \frac{\hbar^2 k^2}{2m} \pm (\alpha + \gamma)|k|$$

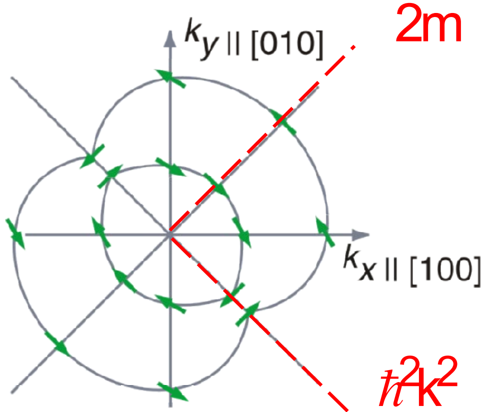

$$E = \frac{\hbar^2 k^2}{2m} \pm (\alpha - \gamma)|k|$$

BIA ≠ SIA

Introduction to spin torques and spin-orbit torques

Magnetization reversal:
"the art of magnetic writing"

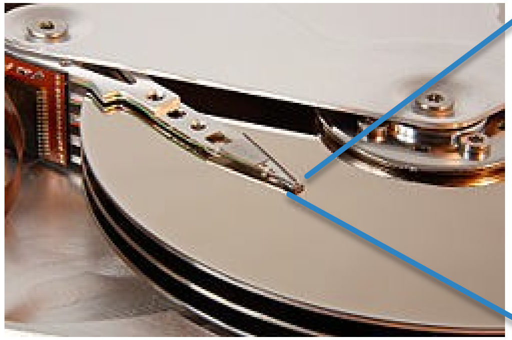

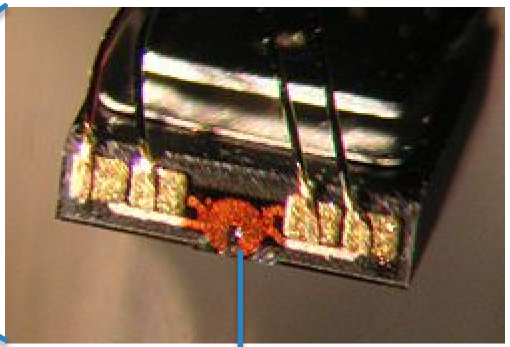

Inductive heads

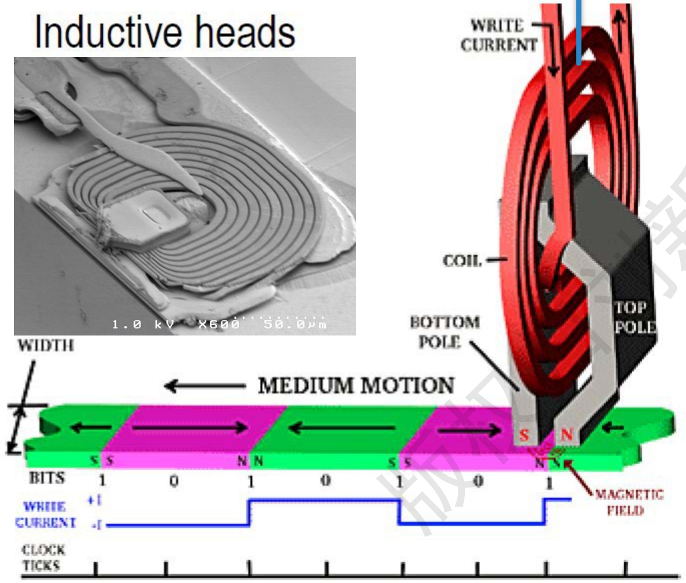

"Mott" two-spin-channel model of ferromagnets

Magnetization switching

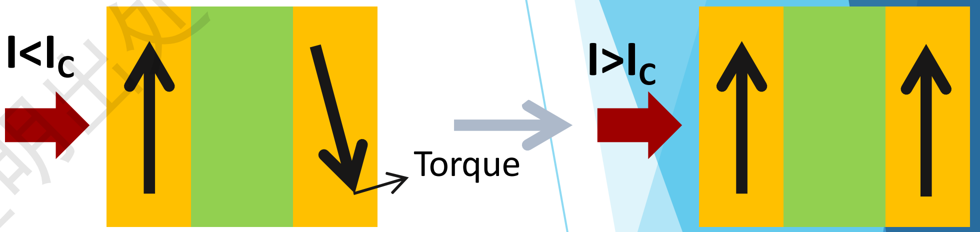

Spin current induced torque

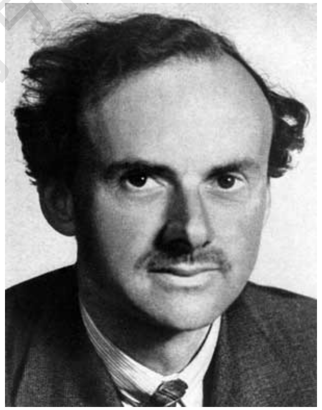

"Dirac" relativistic spin-orbit coupling

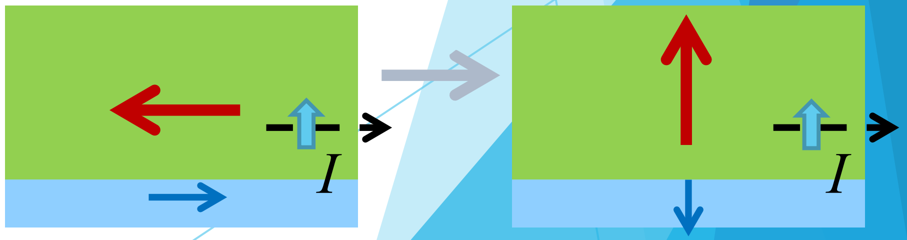

自旋转移力矩、自旋轨道力矩

Writing by current: non-relativistic spin-transfer torque

Spins injected from external polarizer in a non-uniform magnetic structure

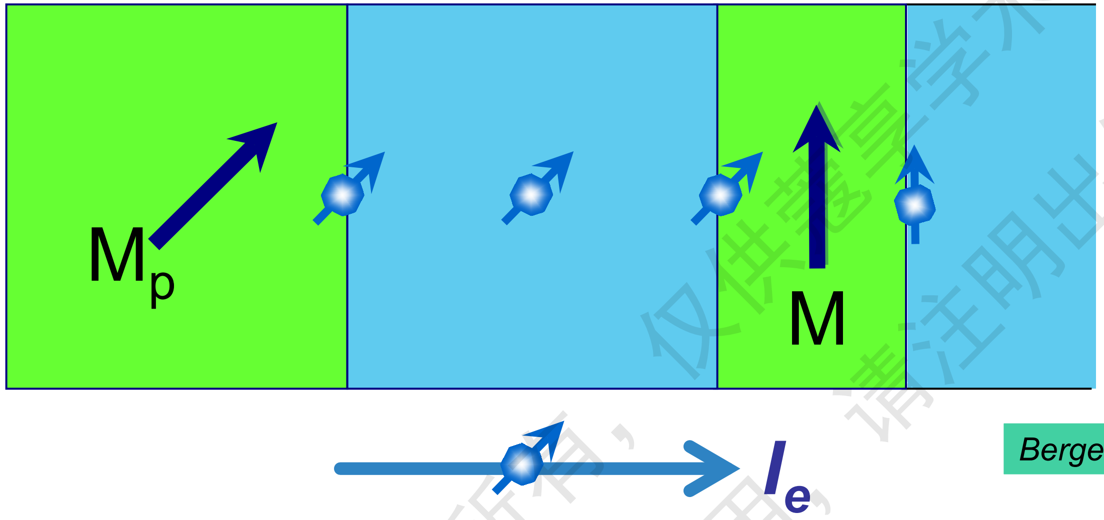

Berger PRB ’96, Slonczewski JMMM ’96

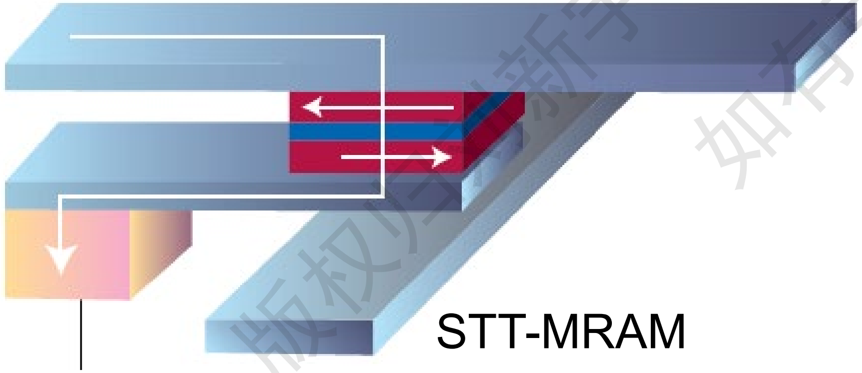

STT-MRAM

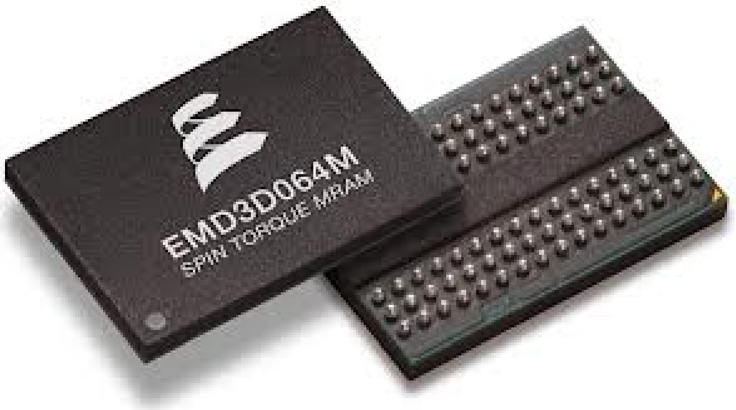

自旋转移力矩

Introducing the STT terms in the LLG equation:

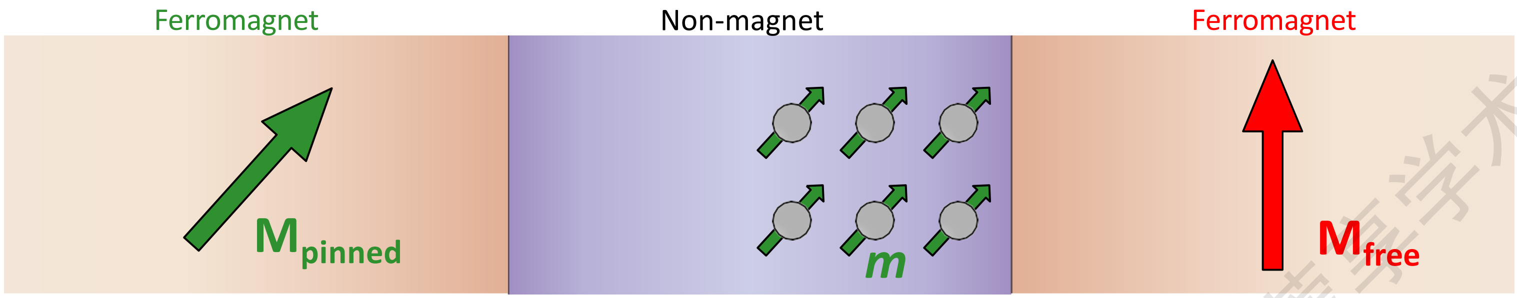

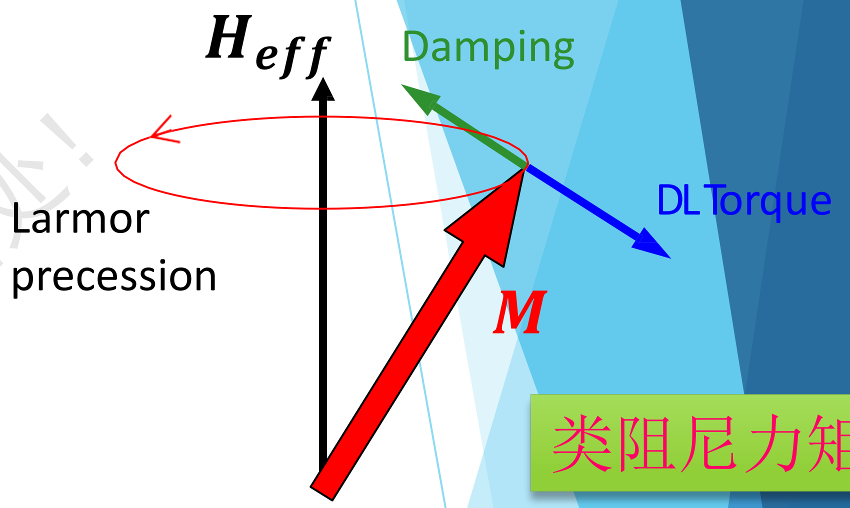

类阻尼力矩

Damping-like (DL) Torque

$$\frac{d\boldsymbol{M}}{dt} = -\gamma_0 \boldsymbol{M} \times \boldsymbol{H_{eff}} + \frac{\alpha}{M_s} \boldsymbol{M} \times \frac{d\boldsymbol{M}}{dt} + \tau_{DL} \boldsymbol{M} \times (\boldsymbol{m} \times \boldsymbol{M}) + (FL)$$

$\boldsymbol{m} = \boldsymbol{m_z}$

Field-like (FL) Torque

$$\frac{d\boldsymbol{M}}{dt} = -\gamma_0 \boldsymbol{M} \times \boldsymbol{H_{eff}} + \frac{\alpha}{M_s} \boldsymbol{M} \times \frac{d\boldsymbol{M}}{dt} + (DL) + \tau_{FL} \boldsymbol{M} \times \boldsymbol{m}$$

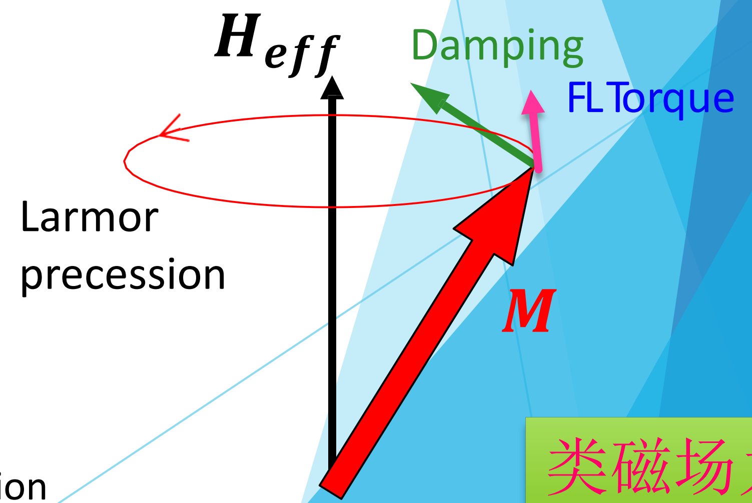

类磁场力矩

Notes: - τ_{DL} and τ_{FL} depend on material (e.g. M_s), geometry, current (***J***)

- $\boldsymbol{m}$ depends on the effect that gave rise to spin accumulation.
Directions of FL and DL torques may be inverted depending on the direction of $\boldsymbol{m}$.
For STT, $\boldsymbol{m} \parallel \boldsymbol{M_{pinned}}$. In some other structures for spintronics, effects arising from spin-orbit coupling, like spin-Hall and Rashba, can give rise to different spin accumulation and torques. These torques are called spin-orbit torques, SOT.

电子自旋与自由层磁矩之间发生自旋角动量的转移

Writing by current: relativistic spin-orbit torque

Spin current in a uniform magnetic structure without external polarizer

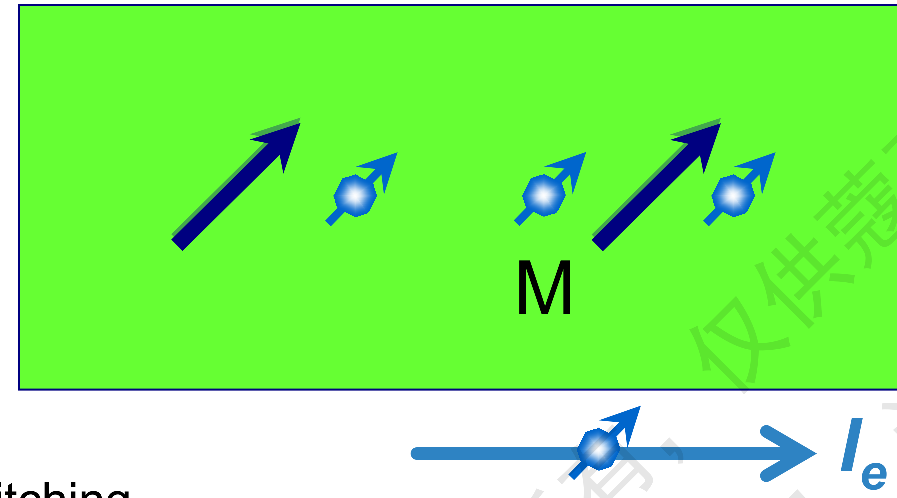

Manchon & Zhang, PRB '08, Chernyshev et al. Nature Phys.'09,
Miron et al. Nature Mater. '10, Fang, Ferguson, TJ et al. Nature Nanotech.'11

In-plane current switching

Miron et al., Nature '11

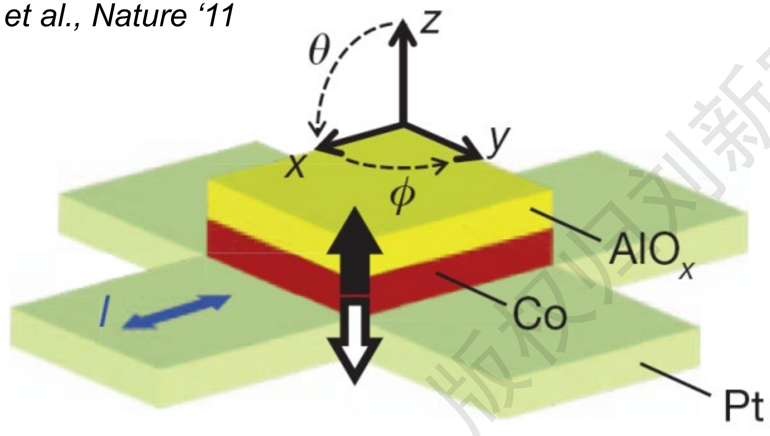

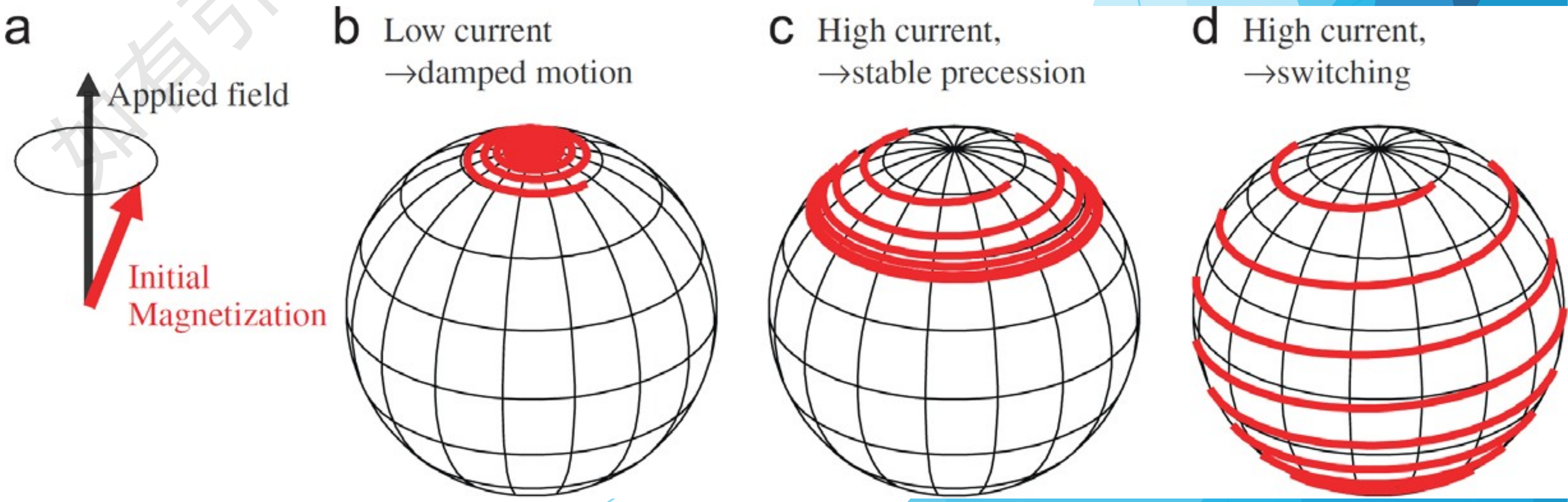

自旋轨道力矩

Reversible control of magnetization by spin-orbit torque

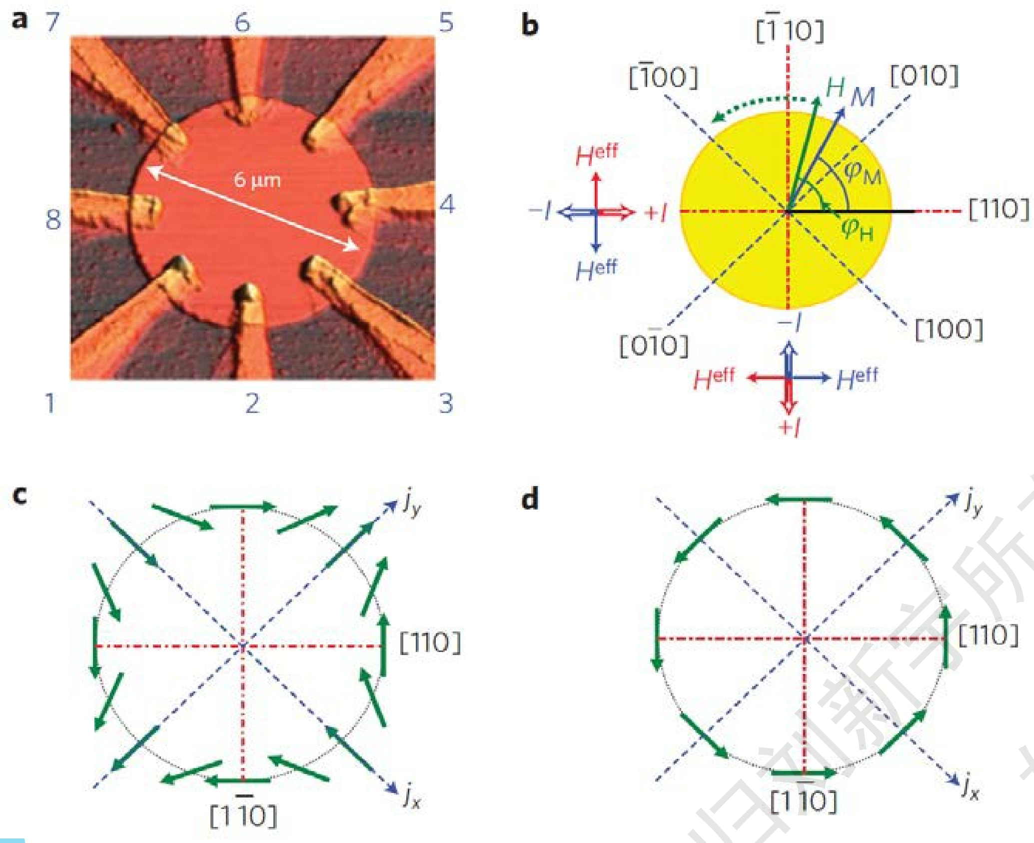

Ga$_{1-x}$Mn$_x$As (6 nm)/GaAs(100)

T = 40 K

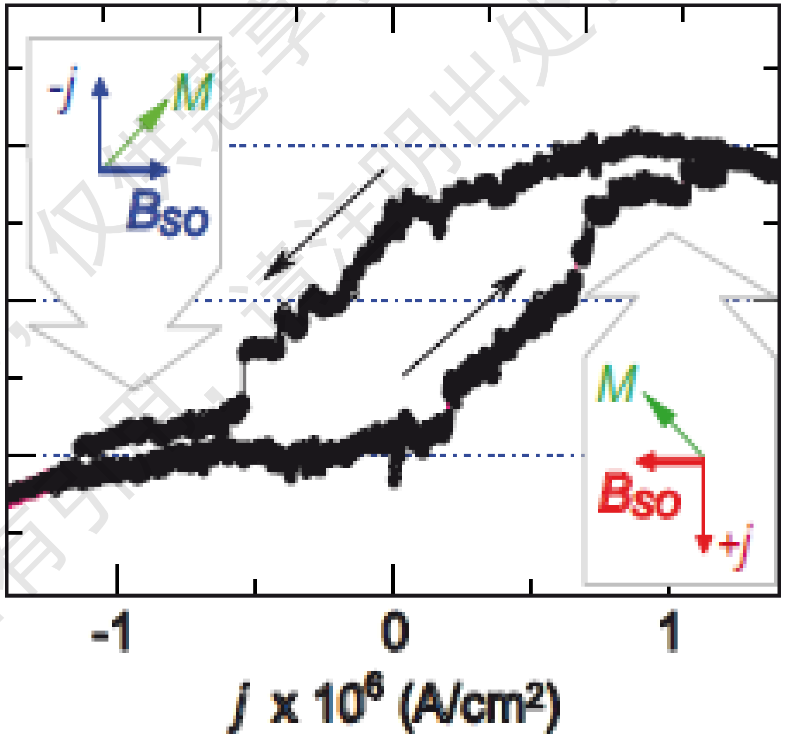

$\Omega_D \propto k^3$ Dresselhaus term

$\Omega_\varepsilon = C\Delta\varepsilon(k_x, -k_y, 0)$ Strain

$\Omega_R = \alpha_R(-k_y, k_x, 0)$ Rashba

Magnetization switching:

AC Hall voltage and AMR modulation

Spin-torque FMR: (Resonant AC current excitation AMR readout)

MOKE

Domain wall motion

Chernyshov et al., Nature Phys. 5, 656 (2009).

铁磁半导体中通过面内电流产生的自旋轨道力矩引起的磁矩翻转

Spin-orbit torque switching in a perpendicular magnet

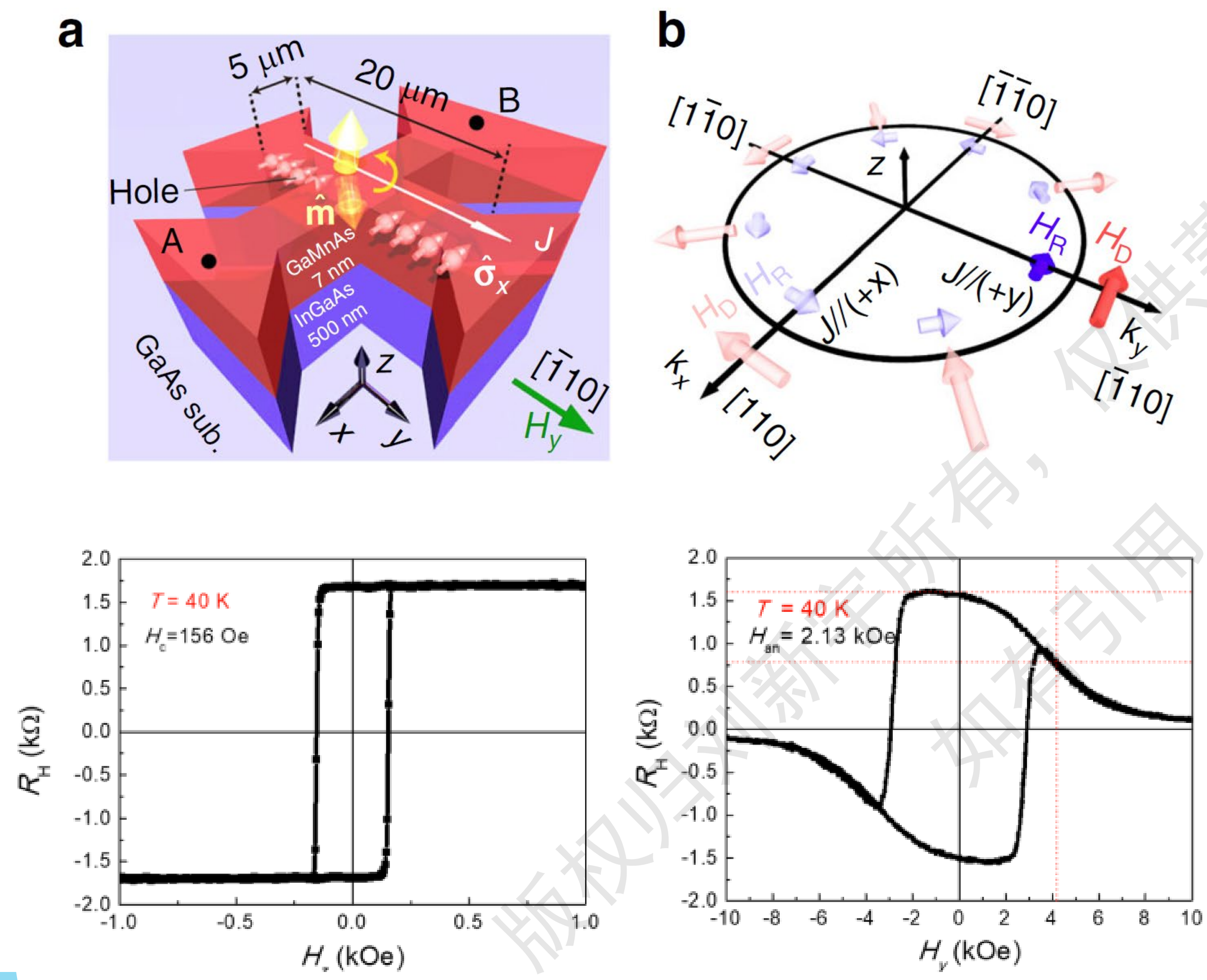

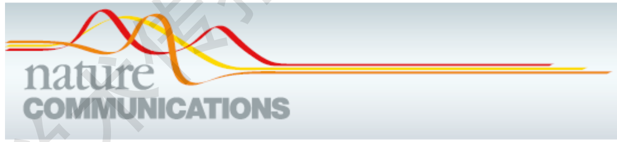

nature COMMUNICATIONS

ARTICLE

https://doi.org/10.1038/s41467-019-10553-x OPEN

Efficient full spin-orbit torque switching in a single layer of a perpendicularly magnetized single-crystalline ferromagnet

Miao Jiang[1], Hirokatsu Asahara[1], Shoichi Sato[1], Toshiki Kanaki[1], Hiroki Yamasaki[1], Shinobu Ohya[1,2,3] & Masaaki Tanaka[1,2]

Spin-orbit torque (SOT), which is induced by an in-plane electric current via large spin-orbit coupling, enables an innovative method of manipulating the magnetization of ferromagnets by means of current injection. In conventional SOT bilayer systems, the magnetization switching efficiency strongly depends on the interface quality and the strength of the intrinsic spin Hall Effect. Here, we demonstrate highly efficient full SOT switching achieved by applying a current in a single layer of perpendicularly magnetized ferromagnetic semiconductor GaMnAs with an extremely small current density of ~3.4×10^5 A cm^{-2}, which is two orders of magnitude smaller than that needed in typical metal bilayer systems. This low required current density is attributed to the intrinsic bulk inversion asymmetry of GaMnAs as well as its high-quality single crystallinity and large spin polarization. Our findings will contribute to advancements in the electrical control of magnetism and its practical application in semiconductor devices.

自旋轨道力矩引起的垂直磁矩翻转

SOT switching and mechanism

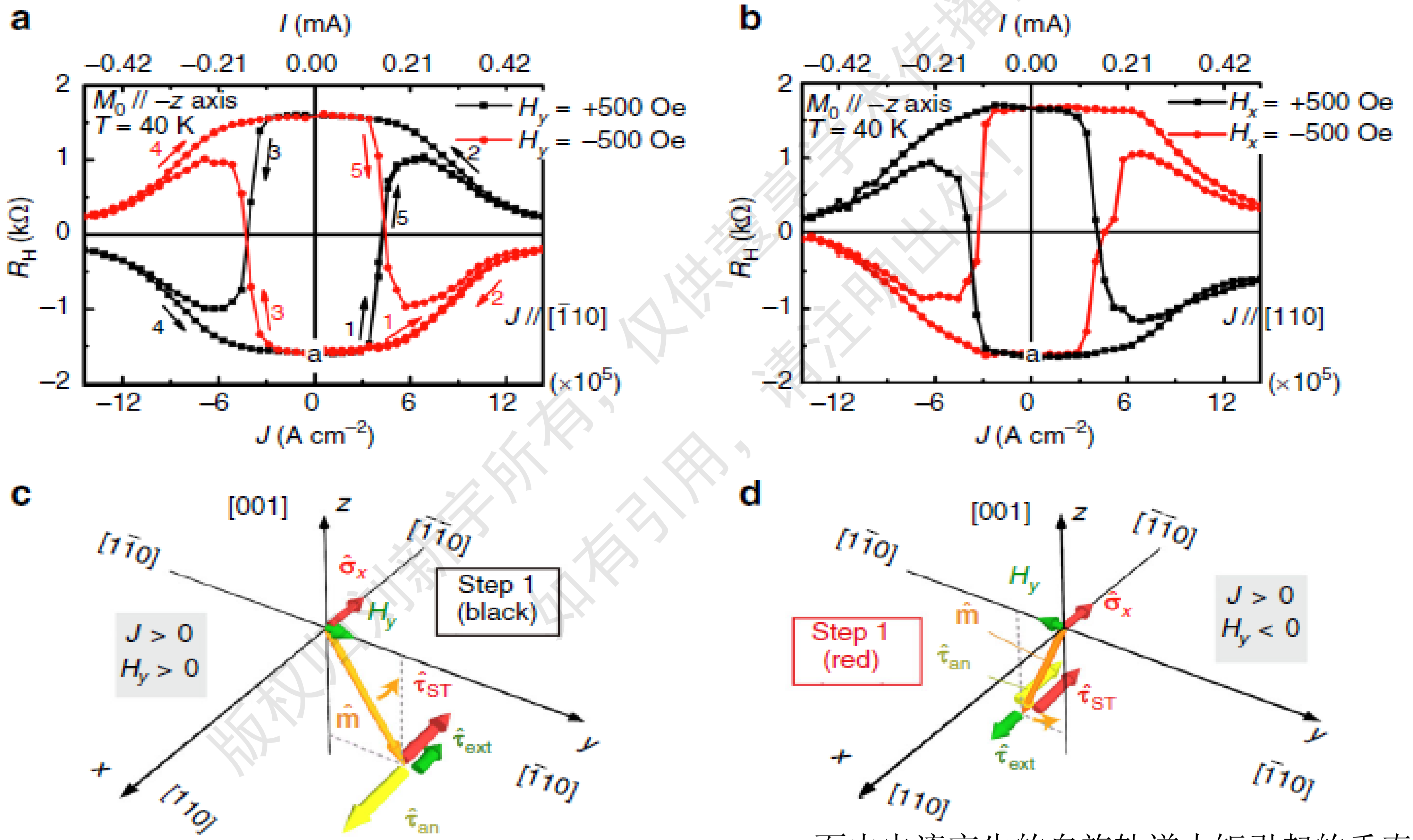

面内电流产生的自旋轨道力矩引起的垂直磁矩翻转

Temperature and Field dependences of SOT switching

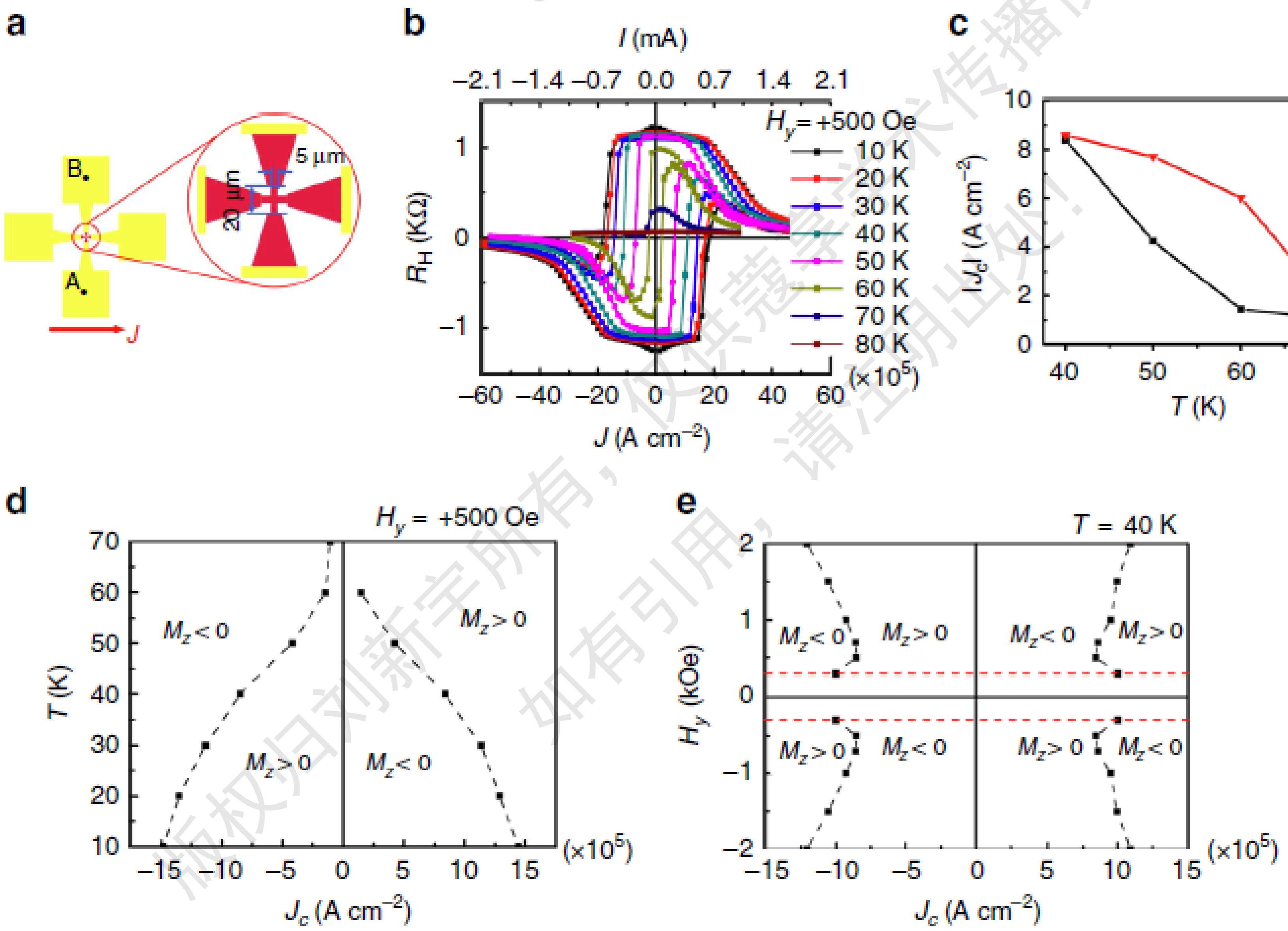

面内电流产生的自旋轨道力矩引起的垂直磁矩翻转

LLG simulation and comparison with experimental results

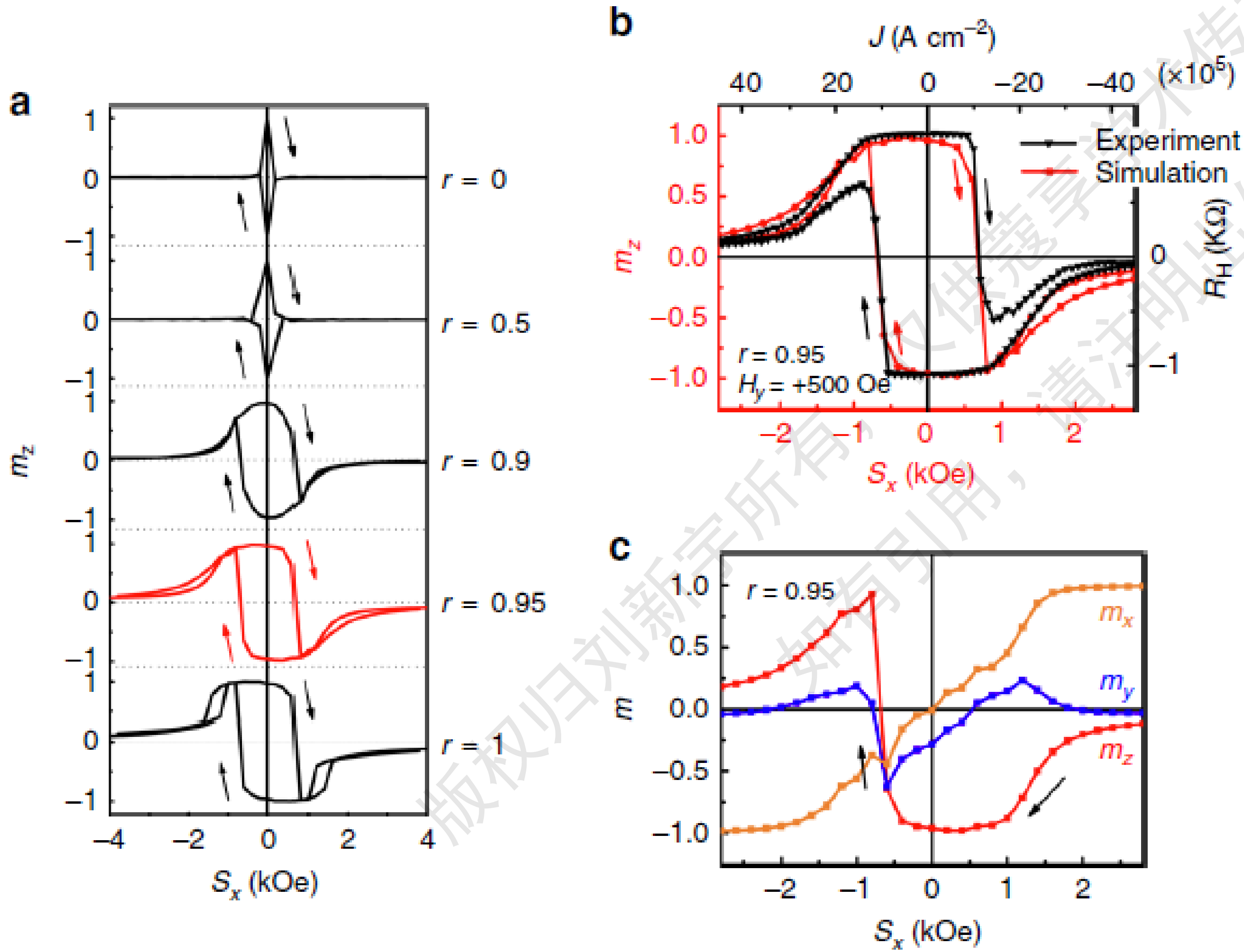

Landau–Lifshitz–Gilbert (LLG) simulation. The obtained $R_H - J$ curves are well reproduced by the LLG equation, which confirms the scenario described above. Here, we consider the SOT switching result obtained at 40 K for the device with metal electrodes as heat sinks (see Fig. 3b) (i.e., J // y with H_y). The LLG equation is expressed as

$$\dot{\hat{\mathrm{m}}} = -\gamma\,\hat{\mathrm{m}}\times\hat{\mathrm{H}} + \alpha\,\hat{\mathrm{m}}\times\dot{\hat{\mathrm{m}}} + \zeta_{\mathrm{DLT}}(\hat{\mathrm{m}}\times\hat{\sigma}_x\times\hat{\mathrm{m}}) + \zeta_{\mathrm{FLT}}(\hat{\sigma}_x\times\hat{\mathrm{m}}), \qquad (1)$$

where $\dot{\hat{\mathrm{m}}}$ is the derivative of $\hat{\mathrm{m}}$ with respect to time; $\hat{\mathrm{H}}$ is the effective field consisting of the external field, the anisotropy field, H_D and H_R; γ is the gyromagnetic ratio; α is the damping constant; ζ_{DLT} is the DLT coefficient; and ζ_{FLT} is the field-like torque (FLT) coefficient. Here, we replace $\zeta_{\mathrm{DLT}}\hat{\sigma}_x$ with $r\gamma\hat{\mathrm{S}}_x$ and $\zeta_{\mathrm{FLT}}\hat{\sigma}_x$ with $\frac{\gamma(1-r)}{\alpha}\hat{\mathrm{S}}_x$, where $\hat{\mathrm{S}}_x$ is the effective magnetic field in the x direction and r expresses the strength of the DLT relative to the total SOT: when r is 0, only the FLT is present, and when r is 1, only the DLT is present. As shown in Supplementary Note 4, the LLG equation can be transformed into

$$\frac{\dot{\hat{\mathrm{m}}}}{\gamma'} = -\hat{\mathrm{m}}\times(\hat{\mathrm{H}}+\beta\hat{\mathrm{S}}_x) - \alpha\hat{\mathrm{m}}\times\hat{\mathrm{m}}\times\left(\hat{\mathrm{H}}+\frac{1}{\alpha}\hat{\mathrm{S}}_x\right), \qquad (2)$$

where

$$\gamma' = \frac{\gamma}{1+\alpha^2},\ \beta = \frac{1-r(1+\alpha^2)}{\alpha}. \qquad (3)$$

SOT switching in a perpendicularly magnetized GaMnAsP

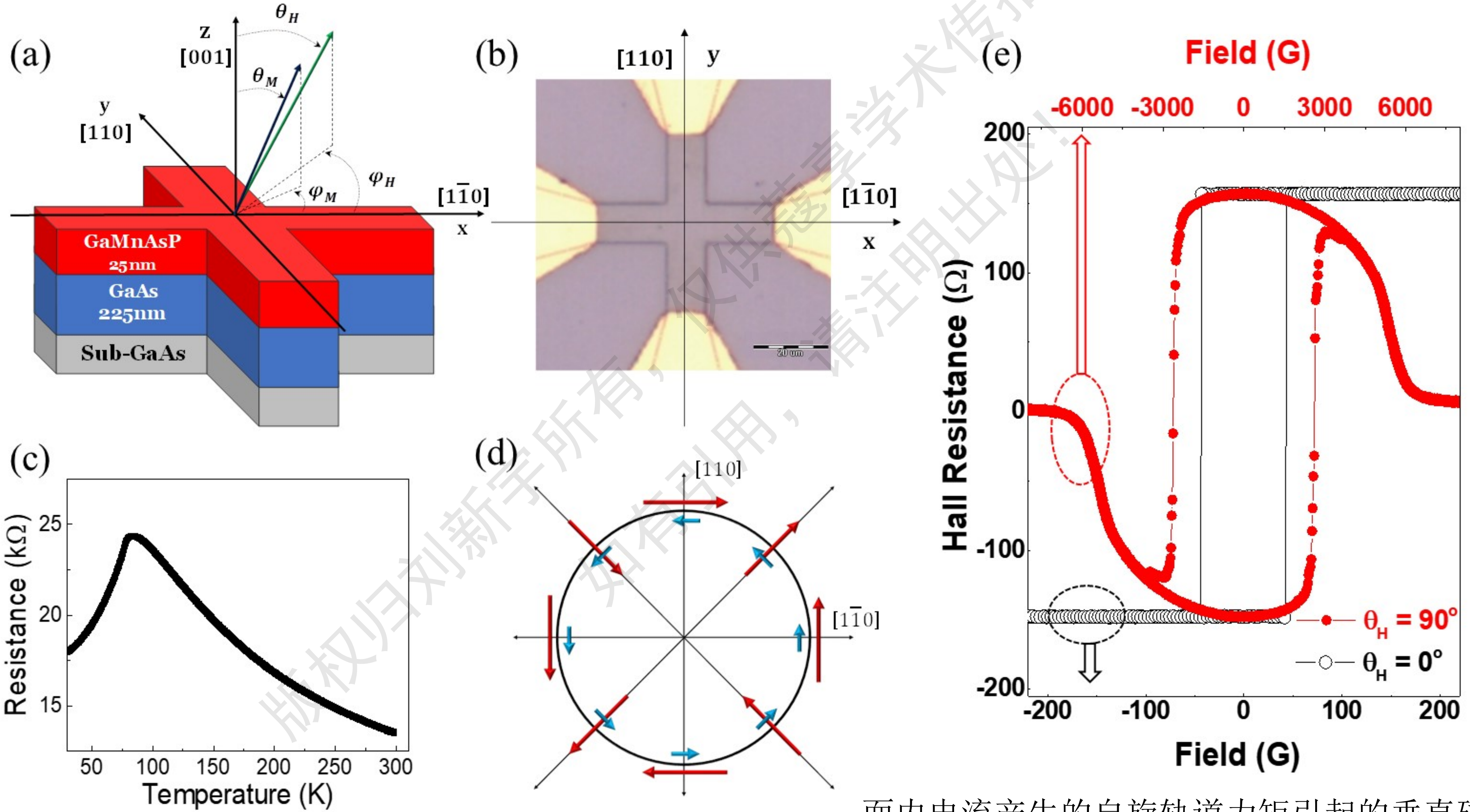

面内电流产生的自旋轨道力矩引起的垂直磁矩翻转

Current induced magnetization switching in GaMnAsP

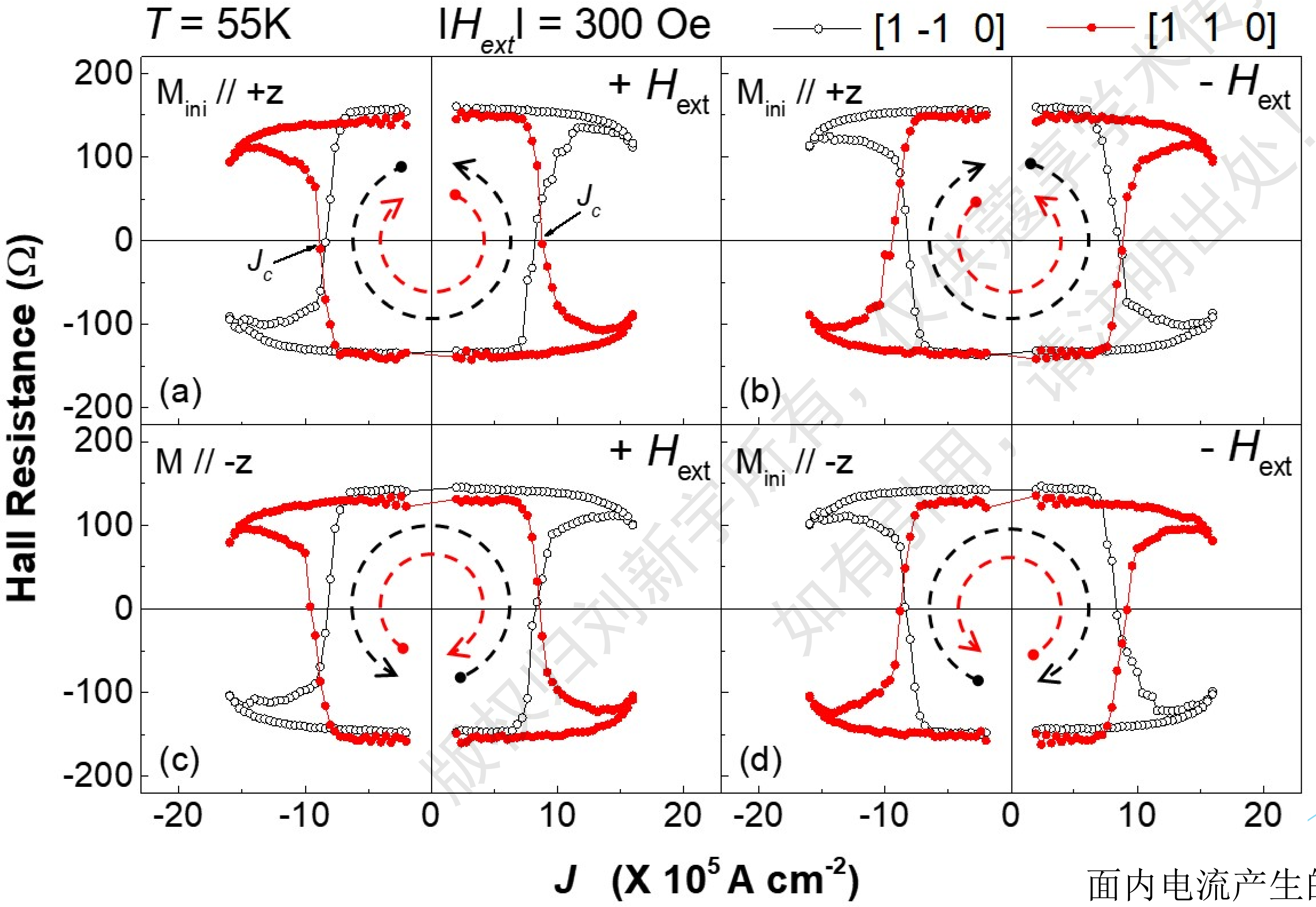

Current induced magnetization switching for the (Ga,Mn)(As,P) film. Hall resistance was measured as a function of current at 55 K for four initial conditions. (a) up magnetization and -300 Oe external field, (b) up magnetization and +300 Oe external field, (c) down magnetization and +300 Oe external field, and (d) down magnetization and -300 Oe external field. Current scan sequences are shown as dotted black (right-hand chirality) and dotted red (left-hand chirality) arrows for the date plotted with open and solid circles, which represent data obtained from the $[1\bar{1}0]$ and the [110] measurements, respectively.

面内电流产生的自旋轨道力矩引起的垂直磁矩翻转

Arrangement of the SO torques in hysteresis loop

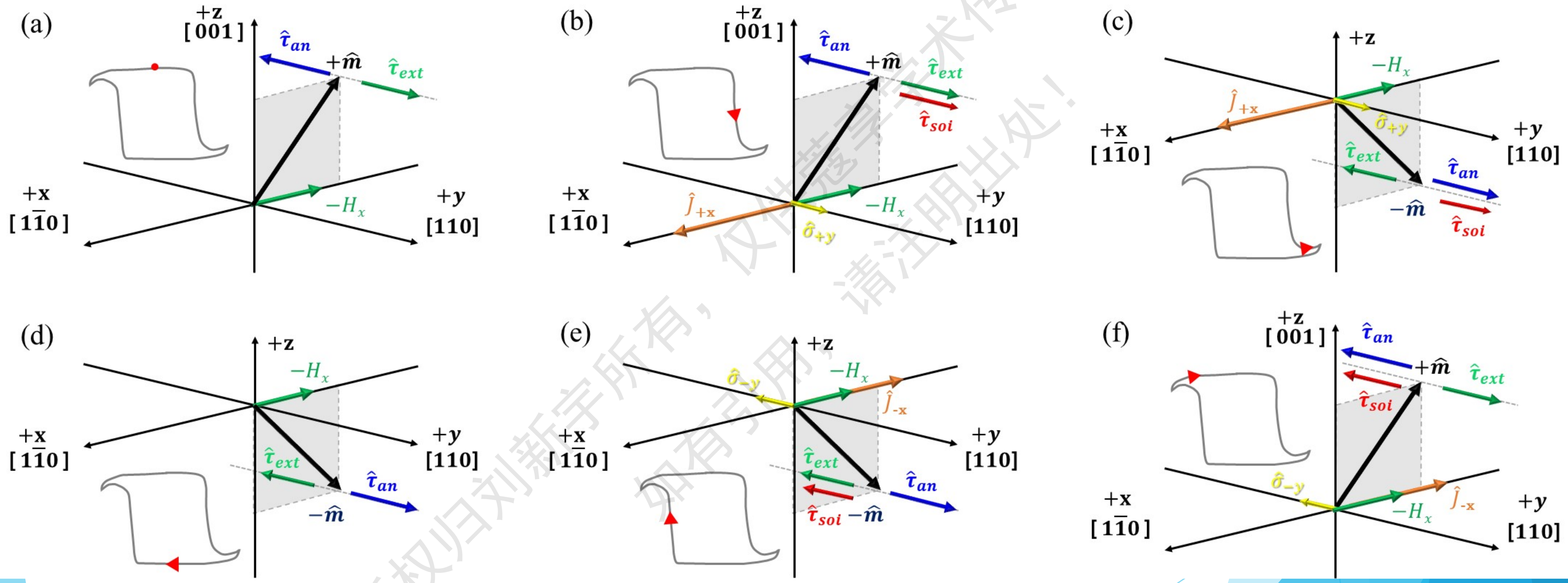

Such current direction dependence of SOI field is a characteristic of the Dresselhaus-type of SOI field in (Ga,Mn)(As,P) film

面内电流产生的自旋轨道力矩引起的垂直磁矩翻转

SOT switching in Zinc-Blende symmetry: [110] vs [1-10]

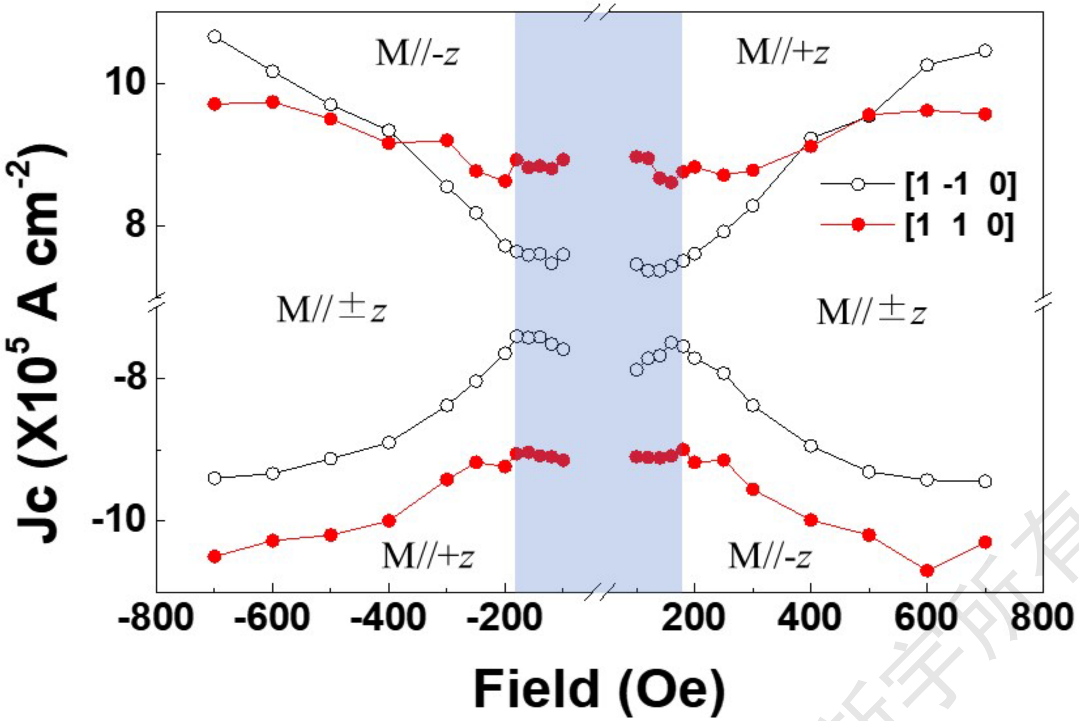

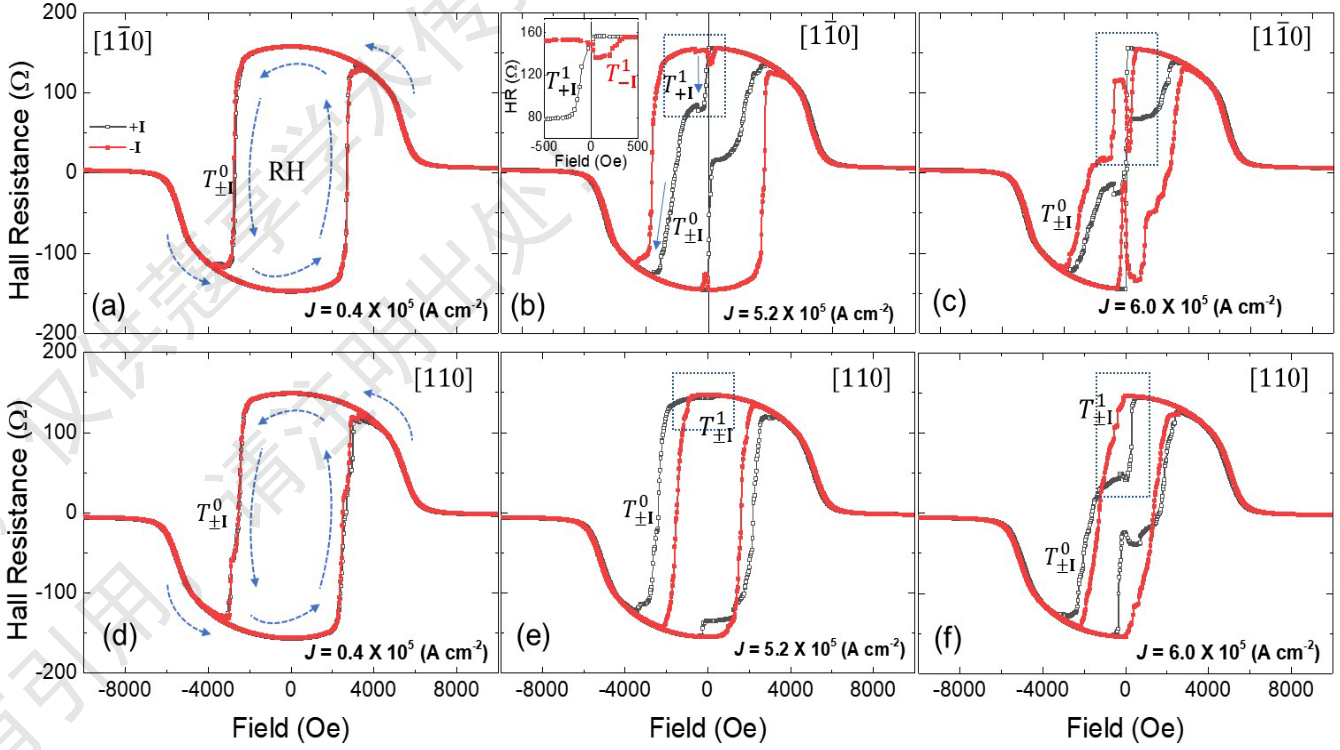

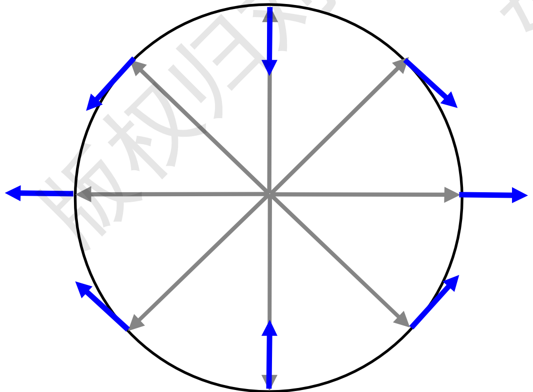

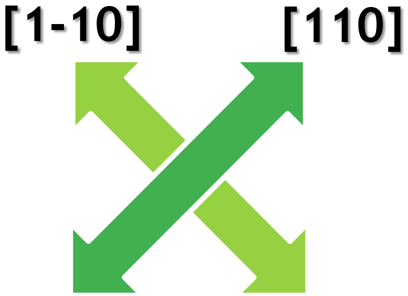

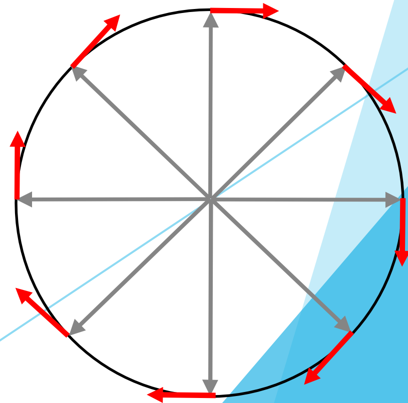

Dresselhaus-type field vs the Rashba-type fields

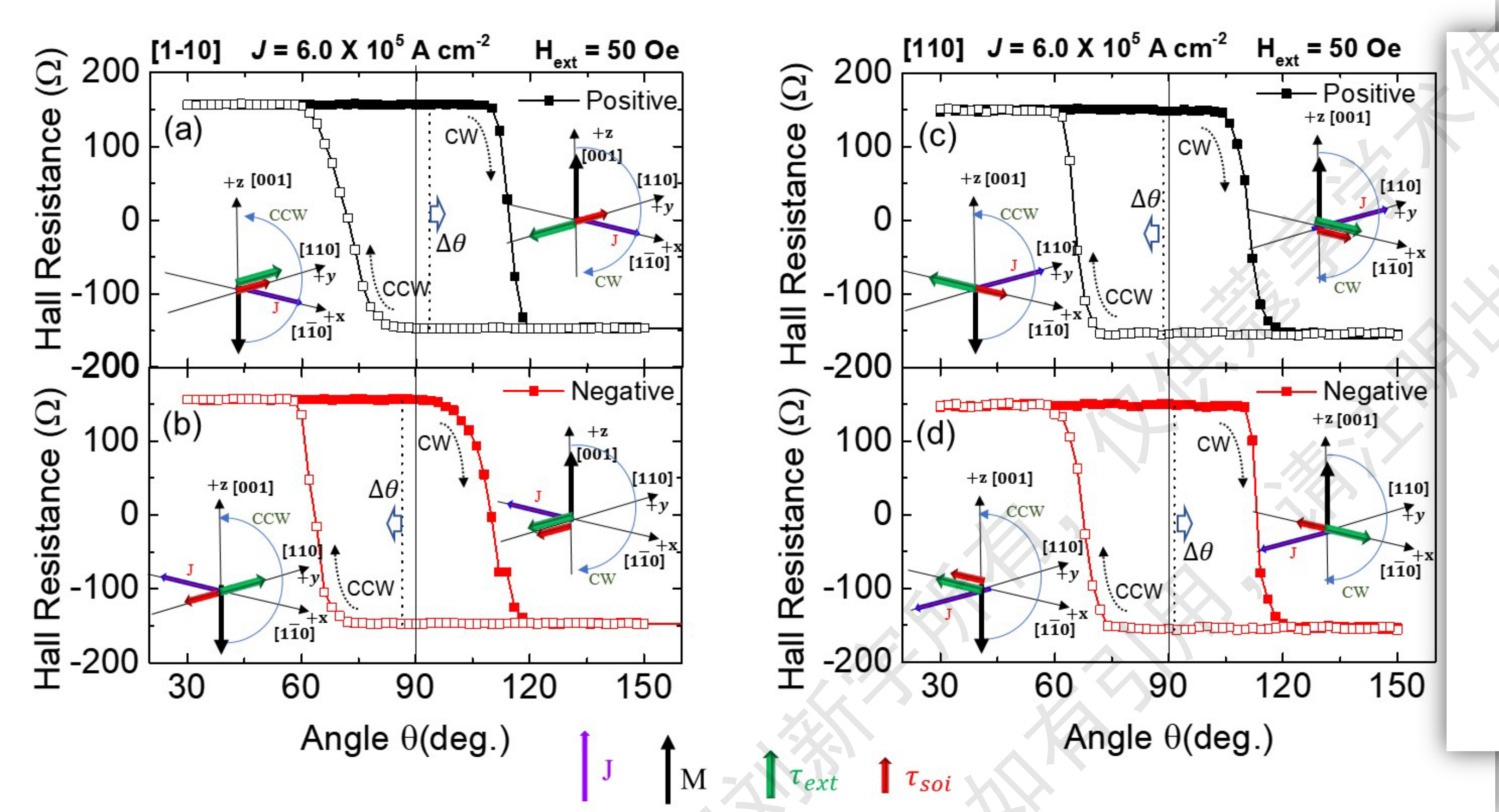

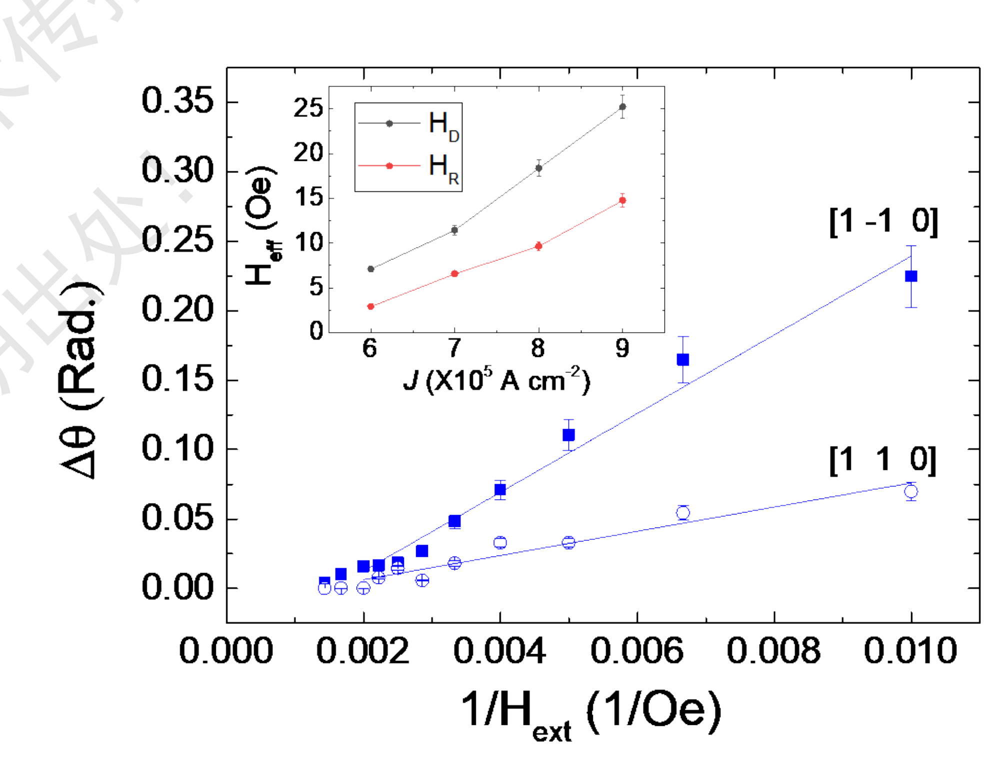

The net SOI field was larger for the [1$\bar{1}$0] current direction than for the [110] current direction, indicating that the Dresselhaus-type field is stronger than the Rashba-type fields in our in a (Ga,Mn)(As,P) film, consistent with current and field scan measurements. The calculated values of Dresselhaus-type and the Rashba-type SOI fields are $H_{eff}^{D} = 13.6$ Oe and $H_{eff}^{R} = 7.5$ Oe, respectively, at the current density of 8.0×10^5 A/cm^2. The Dresselhaus-type and the Rashba-type SOI fields are systematically increases with current density and about 2:1 ratio between two types of fields maintains over all measured current density.

GaMnAsP多层膜中的极端不对称畴壁

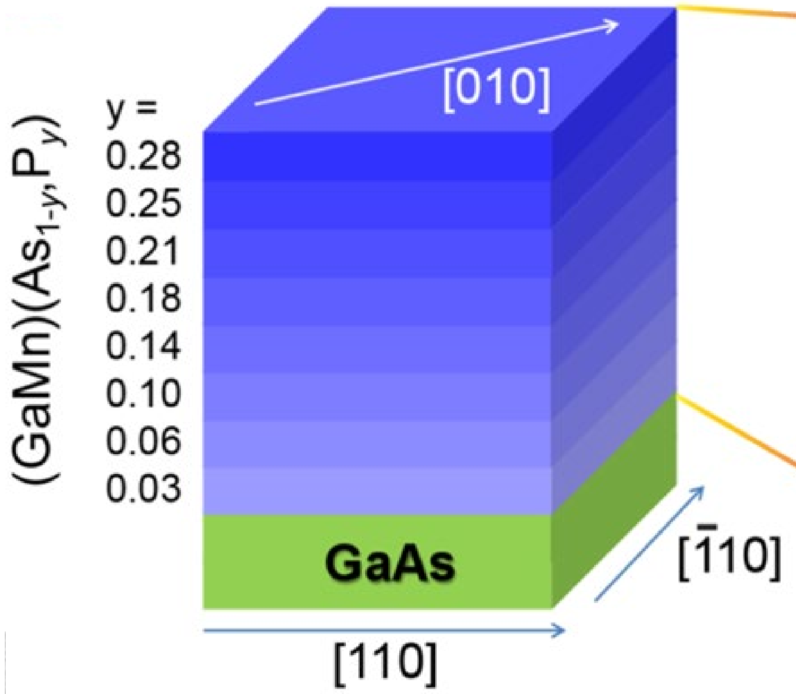

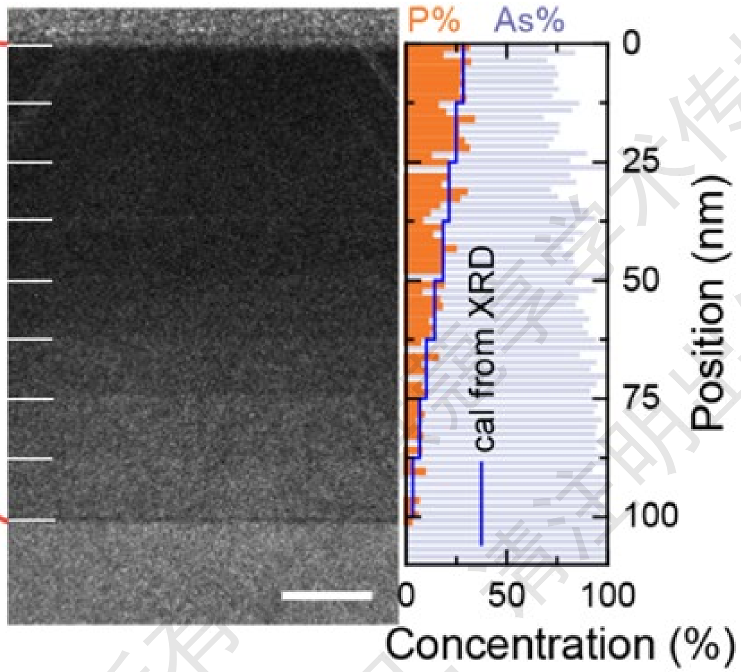

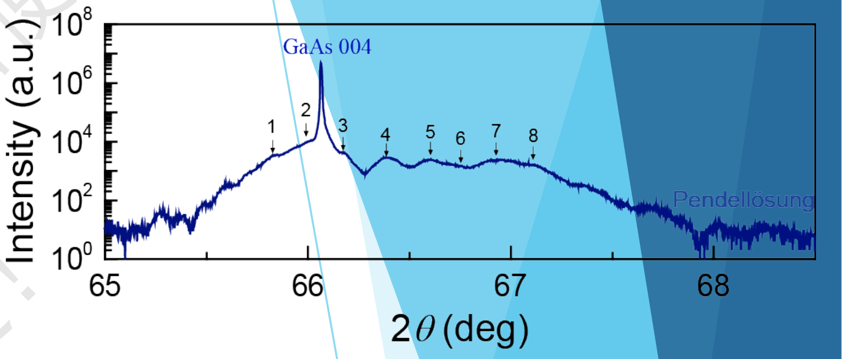

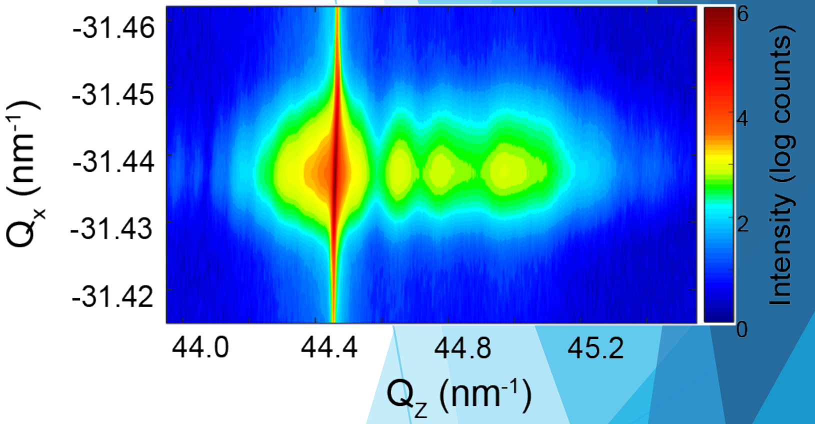

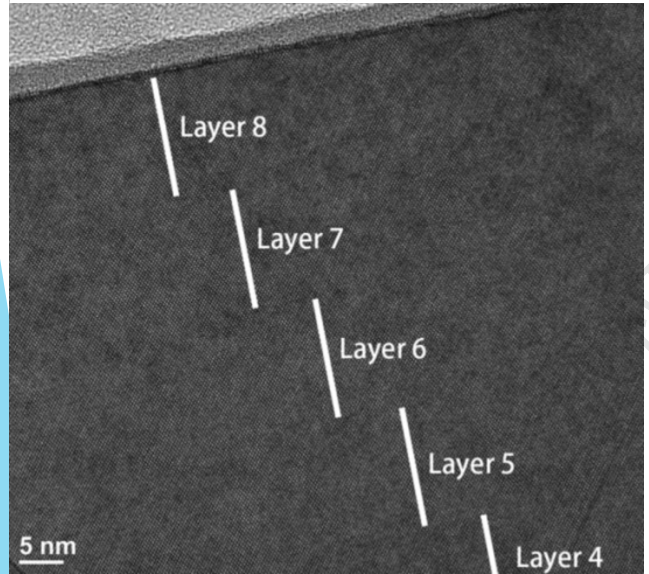

Sketch of the 8-layer graded sample. Dark field TEM image of the sample cross-section (the scale bar is 20 nm). EDX and XRD scans of the As and P concentrations are shown on the right.

Graded Structure

GaMnAsP多层膜中的极端不对称畴壁

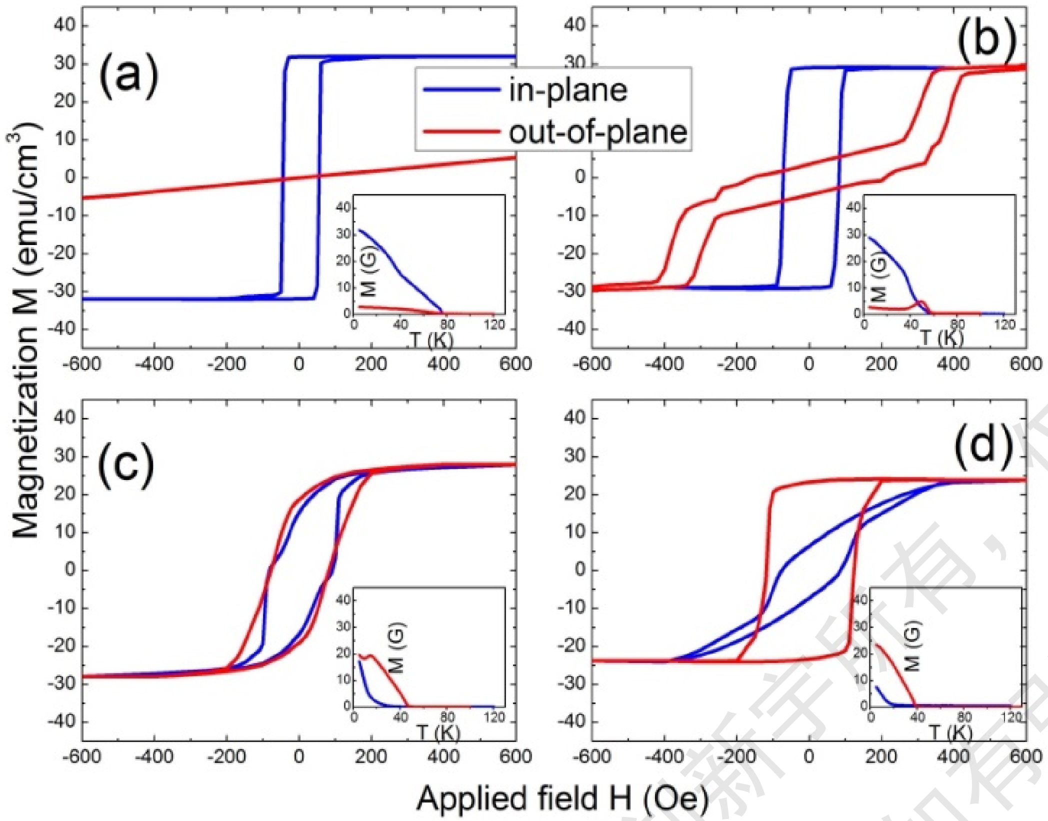

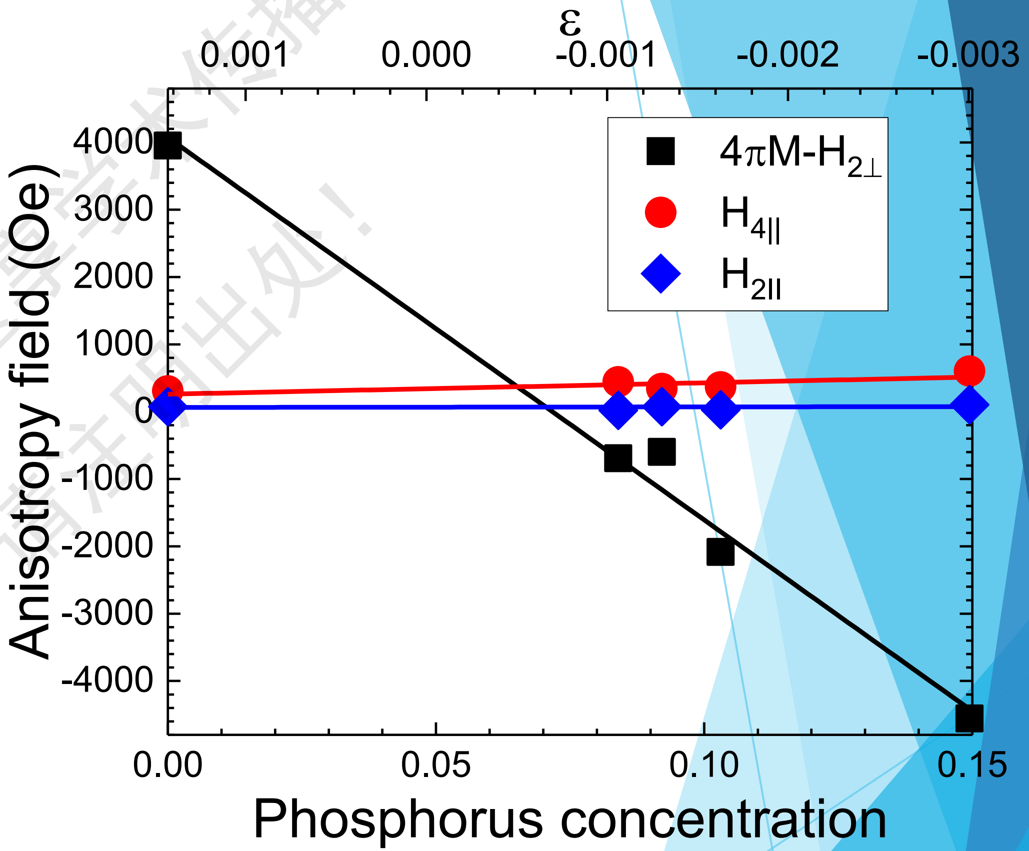

X. Li et al., JVSTB **36**, 02d104, (2018).

Graded Structure

GaMnAsP多层膜中的极端不对称畴壁

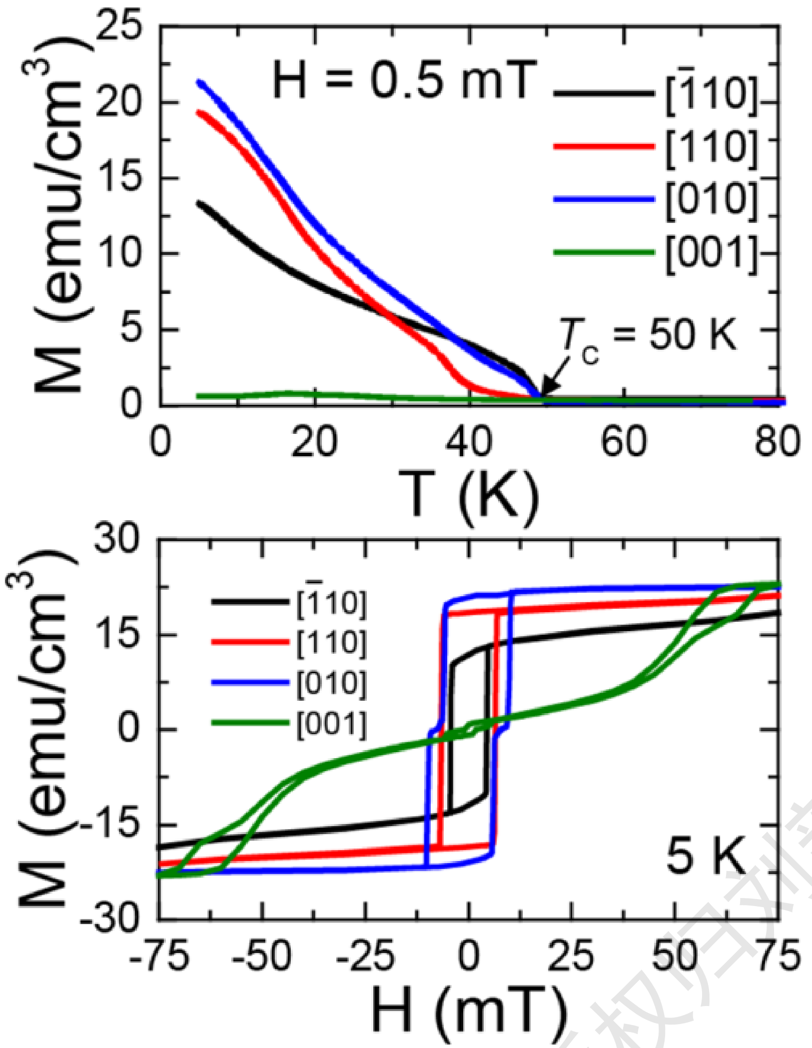

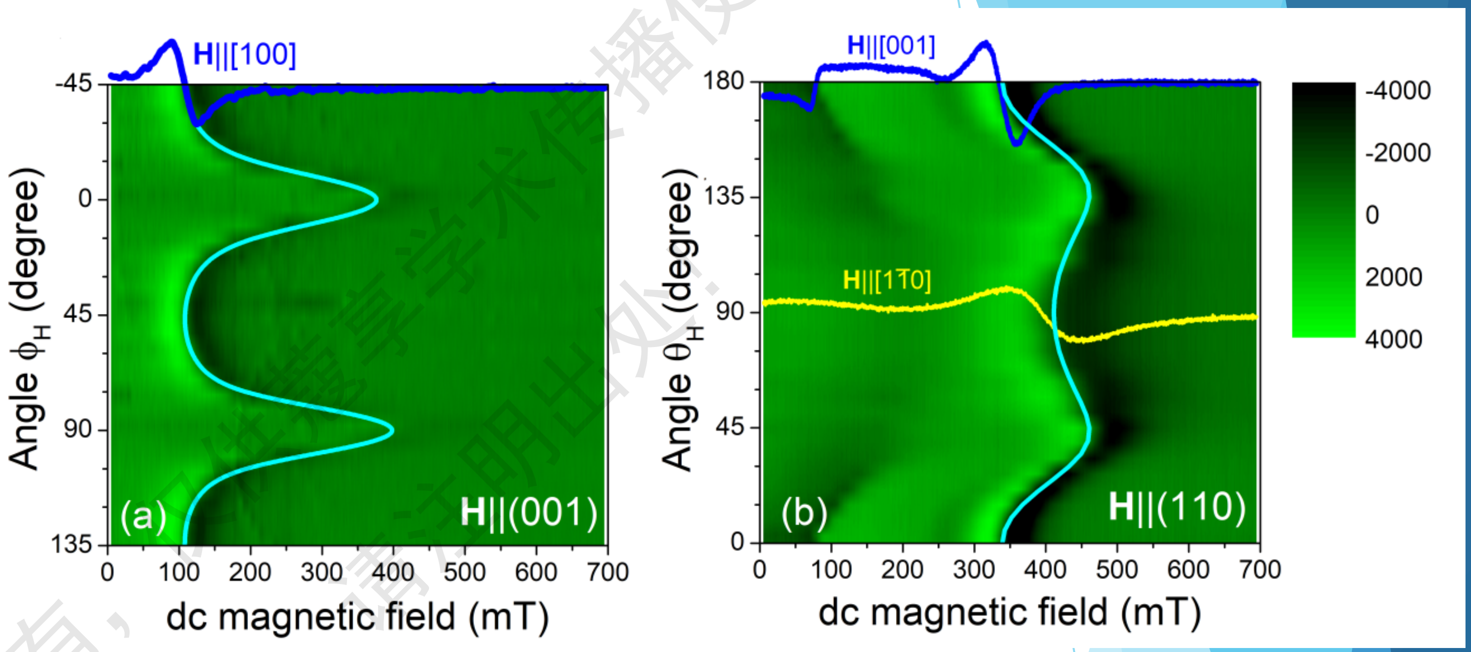

The layers in our graded film are strongly coupled magnetically. As a result, they behave as a single layer film with in-plane magnetization, dominated by the layers close to the substrate, carrying a smaller P concentration, maximum density of the delocalized holes, and compressive strains.

Magnetic characterization

GaMnAsP多层膜中的极端不对称畴壁

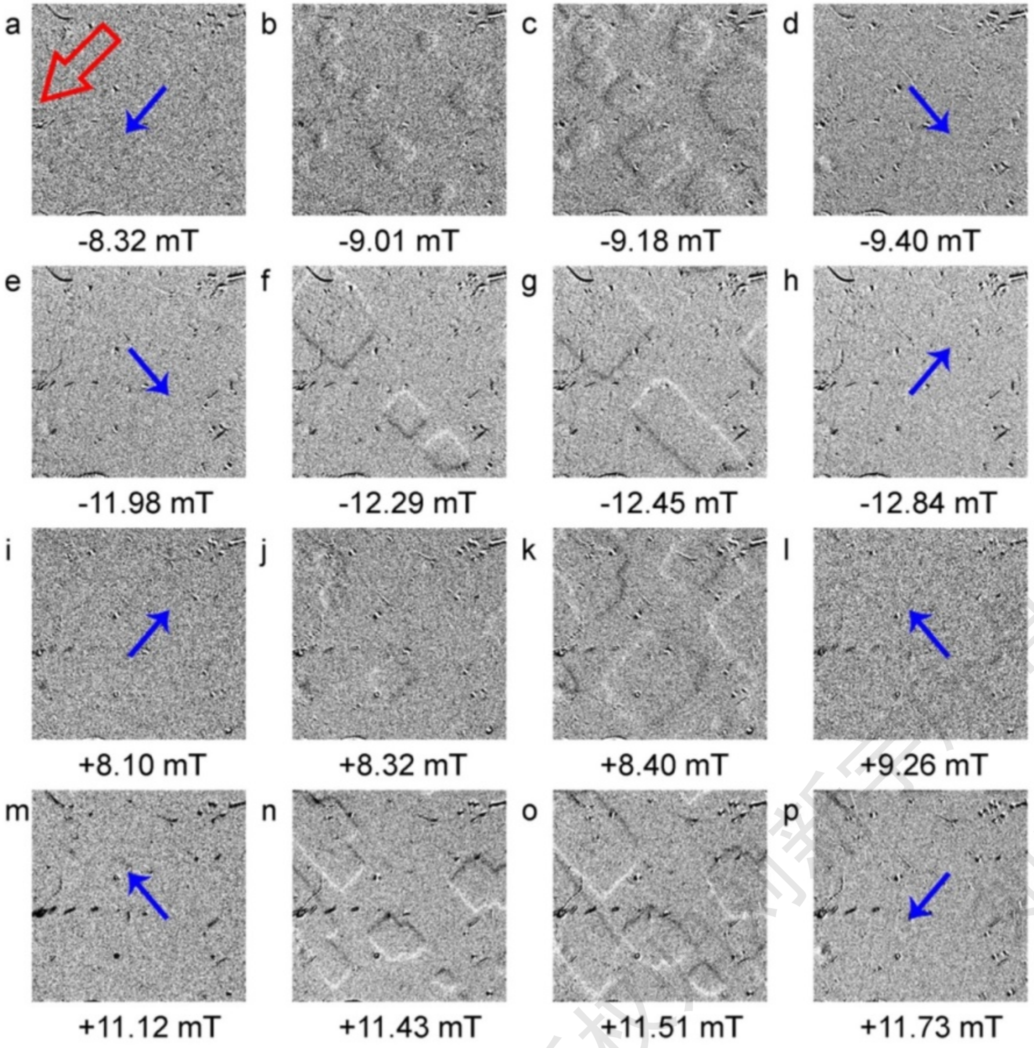

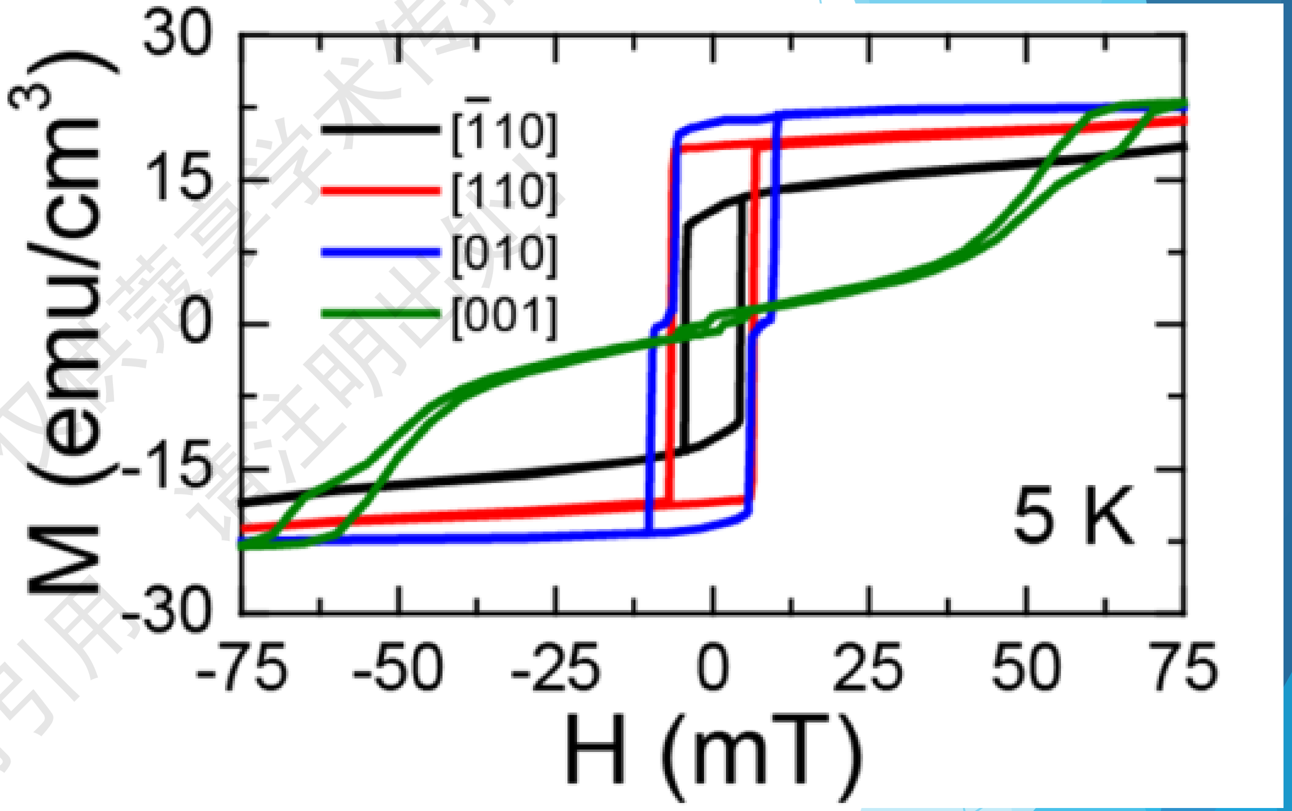

Unique Domain images

GaMnAsP多层膜中的极端不对称畴壁

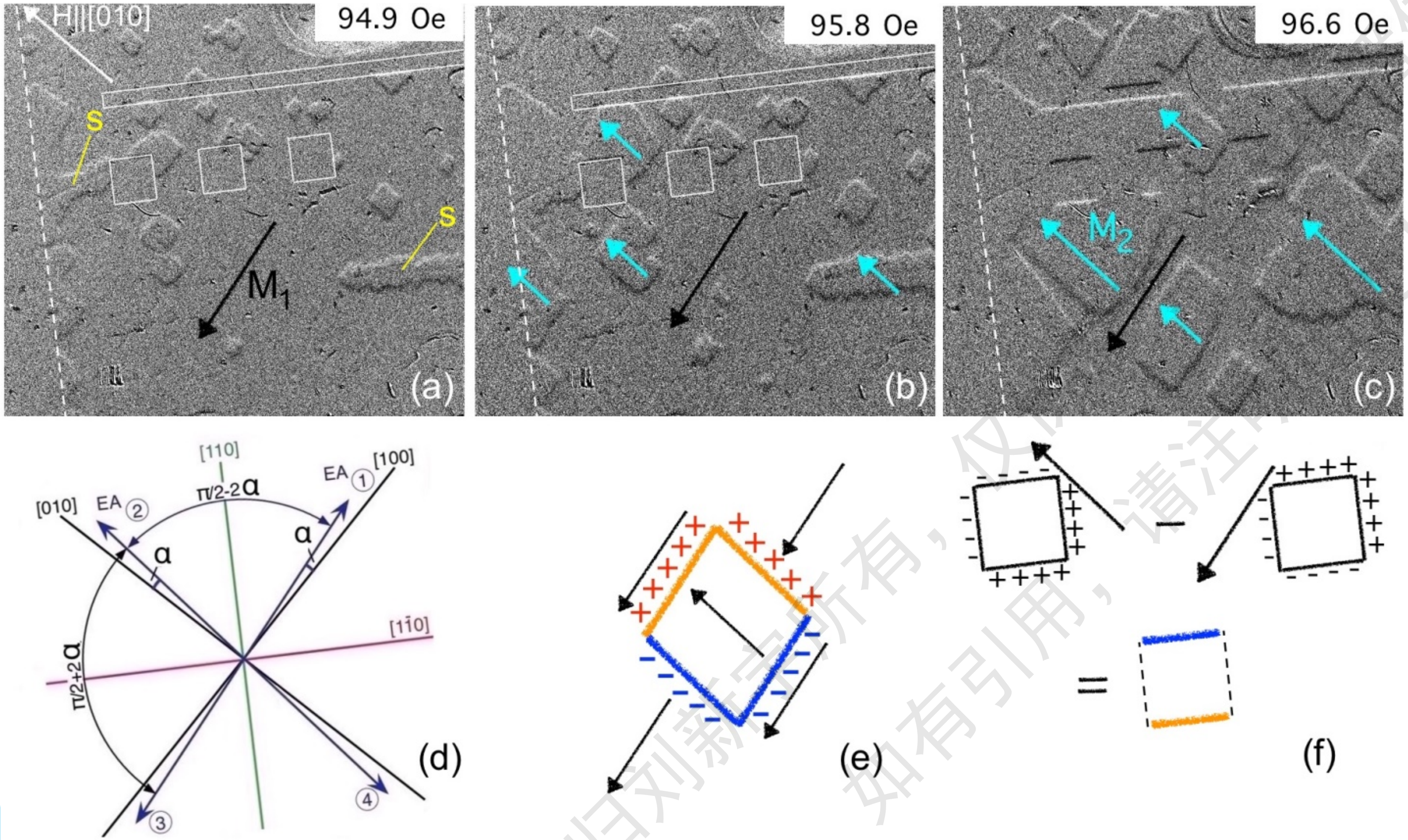

(a)-(c) Magneto-optical images of the nucleation and growth of domains during perpendicular remagnetization at T = 5K. The sample is initially polarized into a mono-domain state (not shown) with $\mathbf{M}_1$||–EA1 (black arrow) by application of $\mathbf{H}$ = 1 kOe||[-100] and switching off H. (a)-(c) present subsequent images in $\mathbf{H}$||[010] after subtraction of the initial polarized $\mathbf{M}_1$ state picture to enhance the contrast of new domains. Rhombus-shaped domains with $\mathbf{M}_2$||EA2 (cyan arrows) appear and grow with increasing H. They have bright and dark 90°+ 2a domain walls (DWs) oriented along EA1 and EA2. The DW bright and dark contrast reveals up and down directed stray fields due to + and – magnetic charges at the DWs (e).

V.K.V. et al., PRB **98**, 180411(R) (2018)

Unique Domain images

GaMnAsP多层膜中的极端不对称畴壁

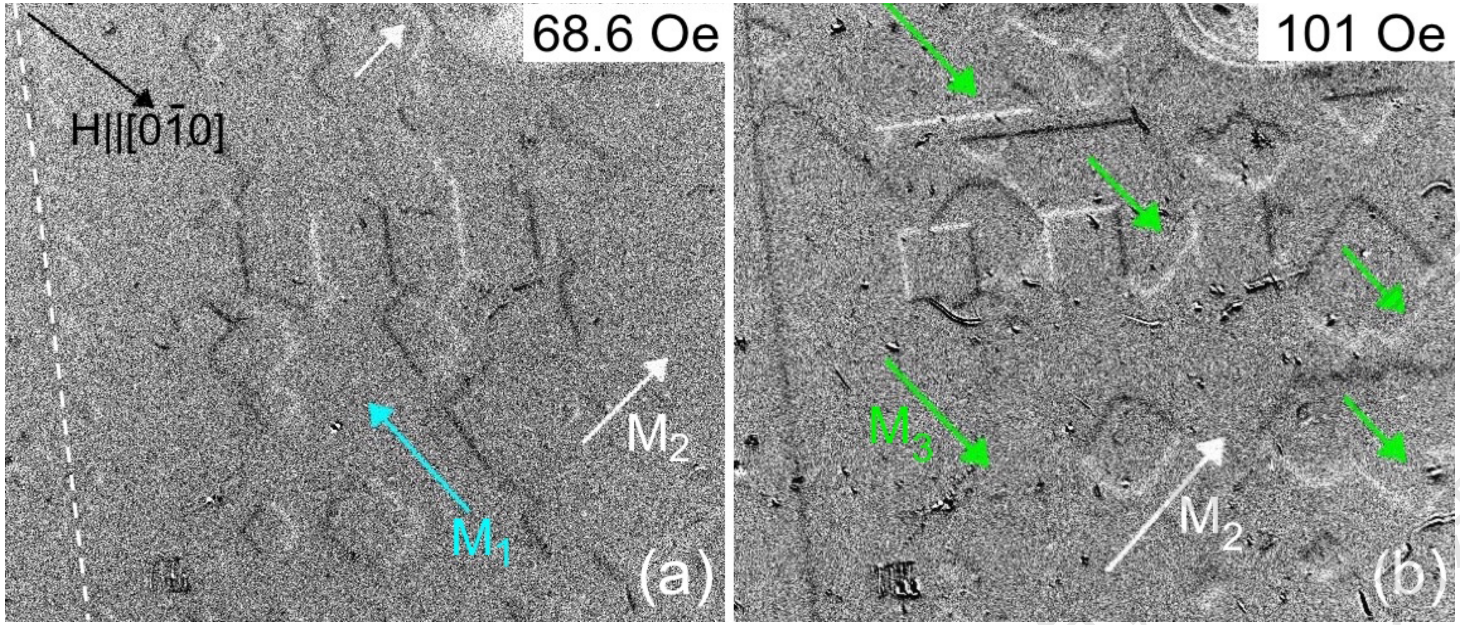

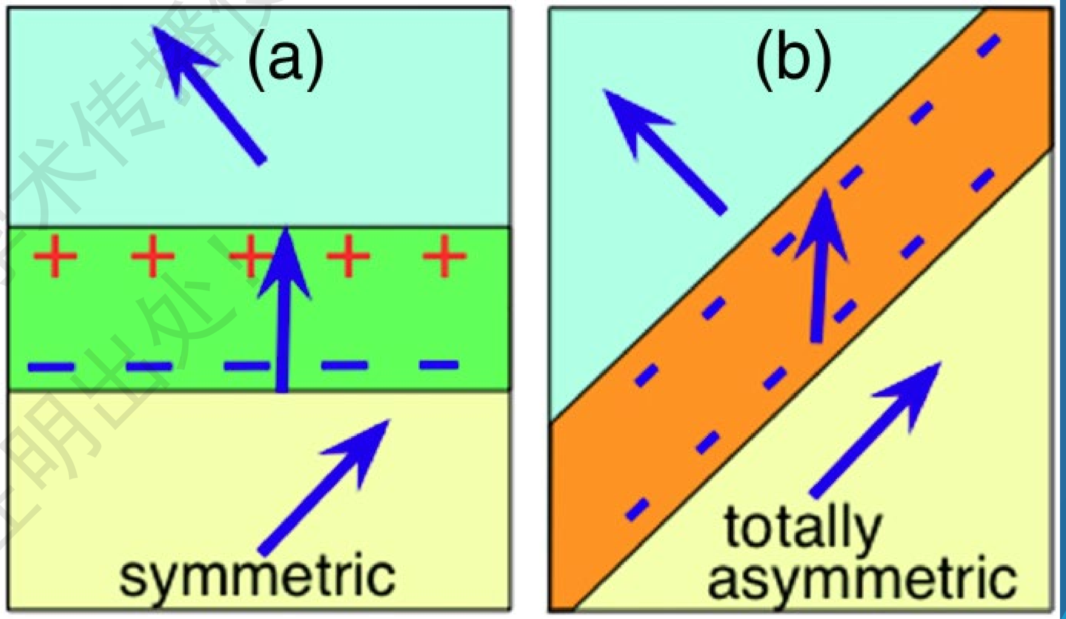

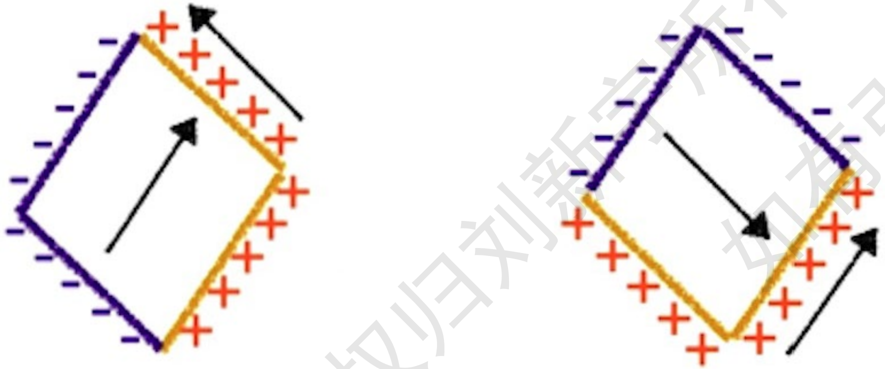

Sketch of symmetric and asymmetric 90° Néel domain walls. (a)-(b) shows the distribution of magnetic charges ρ_m specific for planar Neel walls. In the symmetric case (c), ρ_m changes sign across the DW. However, ρ_m has only one sign (with maximum in the middle of DW) in the asymmetric Neel wall (b), which strongly extends the range of stray fields Hs and increases the resulting magnetostatic energy.

Asymmetry of domain wall

GaMnAsP多层膜中的极端不对称畴壁

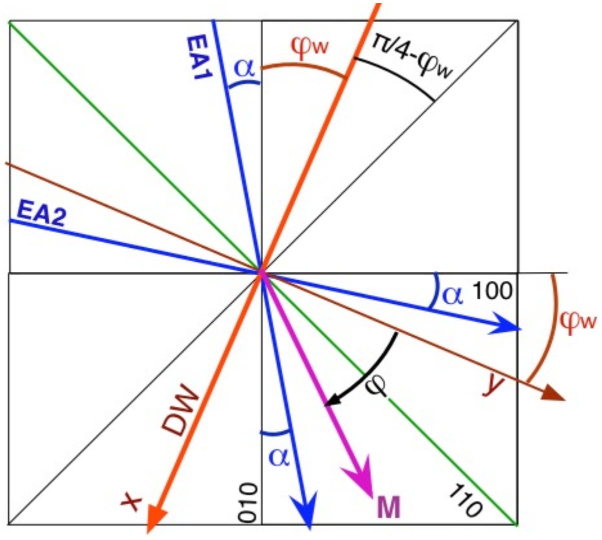

$$E_{DW} = A(d\varphi/dy)^2 + K_c \sin^2 2(\varphi+\varphi_w) + K_u \sin^2(\varphi+\varphi_w - \pi/4) - 1/2 M_y H^s_y$$

$$\frac{y}{\Delta} + C = \frac{1}{2\sqrt{1-\beta^2}} \ln \frac{\sqrt{1-\beta^2} + (\beta u - 1)}{\sqrt{1-\beta^2} - (\beta u - 1)}. \quad (1)$$

Here, y is the coordinate along the DW normal, $\Delta = (A/K_c)^{1/2}$, A is the exchange constant, $\beta = K_u/4K_c = \sin 2\alpha$, K_c and K_u are the cubic and [110] uniaxial anisotropy constants, $u = \tan(\varphi + \varphi_w)$, φ is the angle between **M** and y, φ_w is the angle between y and [100], and $C(\varphi_w)$ gives the position of the DW, which can be chosen, e.g., as $y = 0$ at $\varphi + \varphi_w = \pi/4$, i.e., $u = 1$ in (1).

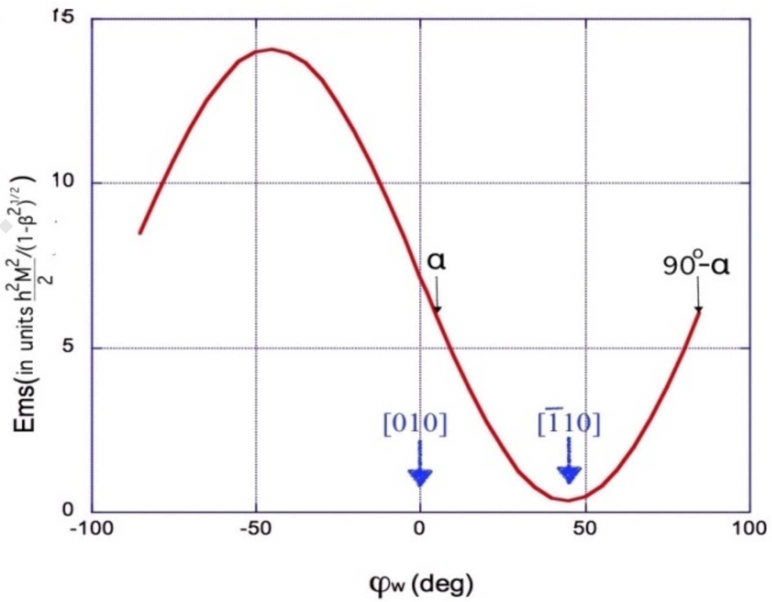

$$\varepsilon_A = \int_{-\infty}^{+\infty} E_A\, dy = \int_{-(\varphi_w-\alpha)}^{\frac{\pi}{2}-\varphi_w-\alpha} E_A\, d\varphi / \frac{d\varphi}{dy} = (AK_c)^{1/2} \int_{-(\varphi_w-\alpha)}^{\frac{\pi}{2}-\varphi_w-\alpha} [\sin 2(\varphi+\varphi_w) - \beta]\, d\varphi =$$

$$= (AK_c)^{1/2}\, [2(1-\beta^2)^{1/2} - \beta\pi/2]$$

$$\varepsilon_{ms} == -h^2 M^2 \int_{-\infty}^{+\infty} \cos\varphi(y)dy \int_{-\infty}^{+\infty} \sin\varphi(y')\left(\frac{d\varphi}{dy}\right)dy'/(y-y')$$

This means that ε_A does not depend on the DW orientation φ_w.

V.K.Vlasko-Vlasov et al., PRB **98**, 180411(R) (2018)

Micromagnetic Analysis

GaMnAsP多层膜中的极端不对称畴壁

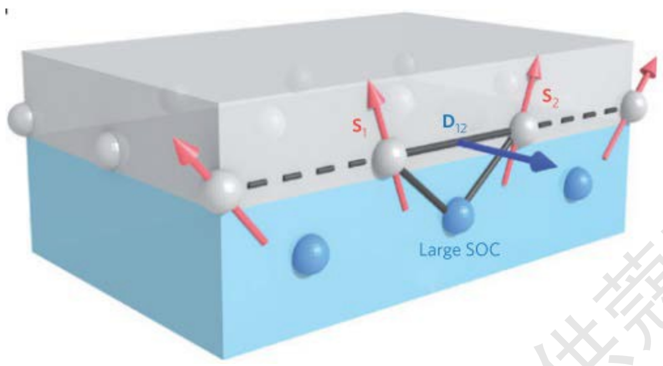

$$H_{DM} = D_{ij}\left(\mathrm{S_i} \times \mathrm{S_j}\right)$$

A.I. Liechtenstein *et al.* JMMM **67** (1987) 65,
M. Heide *et al.* Spin Orbit Driven Physics at Surfaces
S. Meckler *et al.* Phys. Rev. B **85** (2012) 024420
A. Fert *et al.* *Nat.* Nanotec. **8** (2013) 152

Infinite stripe: $D < D_c = \sqrt{A/K}$ collinear

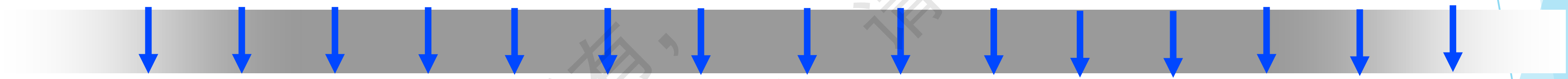

Infinite stripe: $D > D_c$ spiral

Finite stripe: $D < D_c$ canted

Dzyaloshinskii-Moriya interactions

GaMnAsP多层膜中的极端不对称畴壁

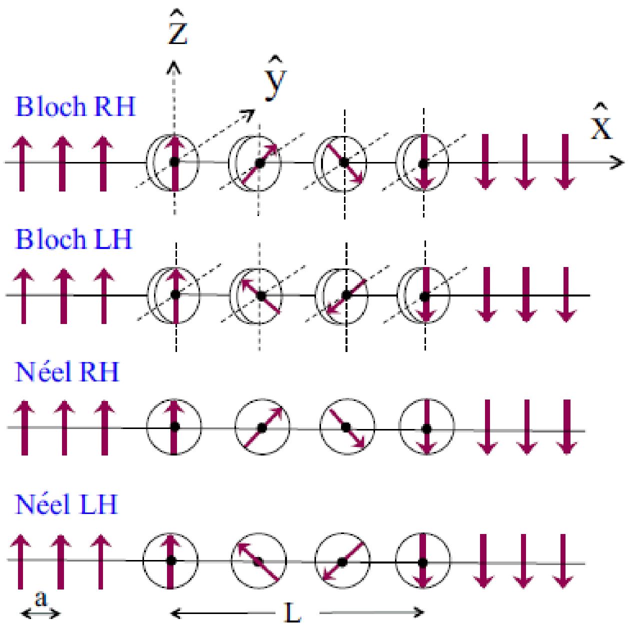

FIG. 6. Bloch and Néel walls, right (RH) and left (LH) handed.

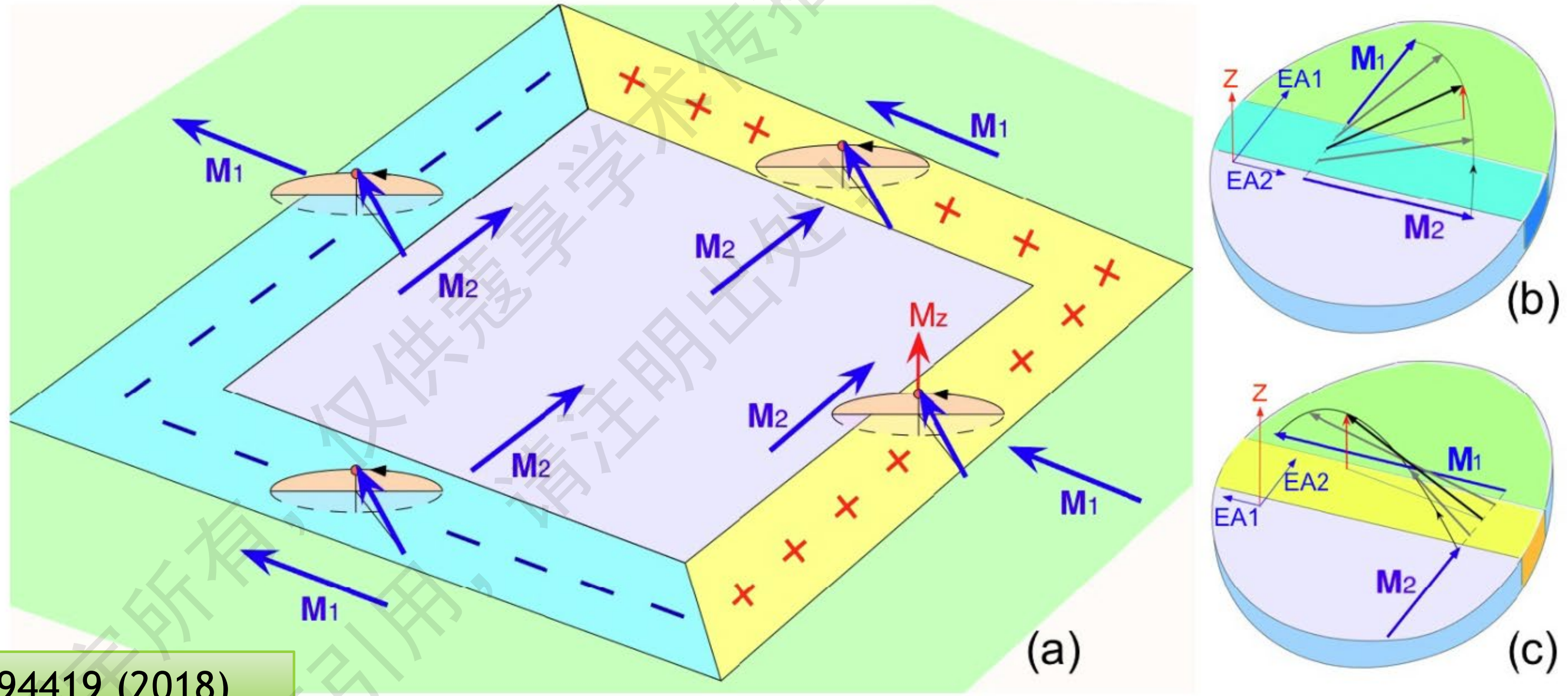

M. M. VALIZADEH & S. SATPATHY PRB **97**, 094419 (2018)

Due to the DMI, magnetization in the Néel DW tilts slightly out of the plane, as shown by ellipses with their small axis along the film normal Z. Within the DWs, M rotates in the film plane and out of plane as shown in (b) and (c). Magnetic charges in the DWs shown by + and − are defined by the asymmetric in-plane rotation of M. All the DWs around the nucleating domain have the same CCW chirality for rotation from M2 to M1.

Dzyaloshinskii-Moriya interactions

Summary of Spin-Orbit Interaction

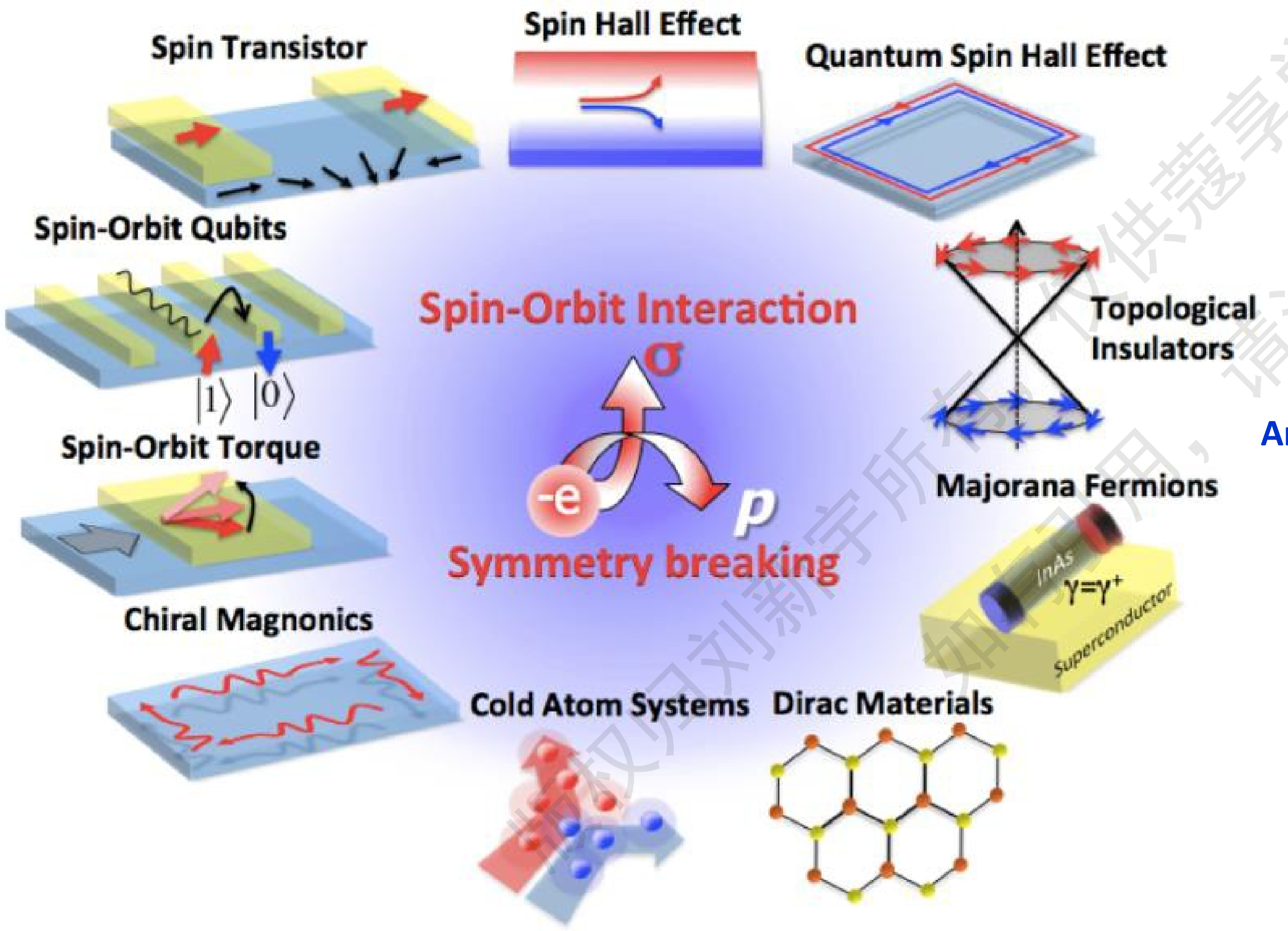

Intended applications:

- Information technology-IT (e.g. memory, processors, data security)
- Biomedical (e.g. sensors)
- Telecommunication-T (e.g. transceiver)
- Artificial intelligence-AI (e.g. neuromorphic computing)

Among current research topics:

- Topology
- Transfer of angular momentum: electron, phonon, photon
- Terahertz spectroscopy and technology
- ‘New’ materials / structures / instrumentation
- Spintronics
- Mature fields: MRAM/Design (IT), Sensors (IT, Bio), Oscillators (T, AI)

Thank!

Vitalii K. Vlasko-Vlasov and Wai-Kwong Kwok

Materials Sciences Division, Argonne National Laboratory, Argonne, Illinois 60439, USA

Sining Dong

Research Institute of Superconductor Electronics, School of Electronic Science and Engineering, Nanjing University, Nanjing 210093, China

Sanghoon Lee

Physics Department, Korea University, Seoul 136-701, Republic of Korea

Margaret Dobrowolska and Jacek K. Furdyna

Physics Department, University of Notre Dame, Notre Dame, IN 46556, USA

U.S. DEPARTMENT OF ENERGY

Length- and energy-scales

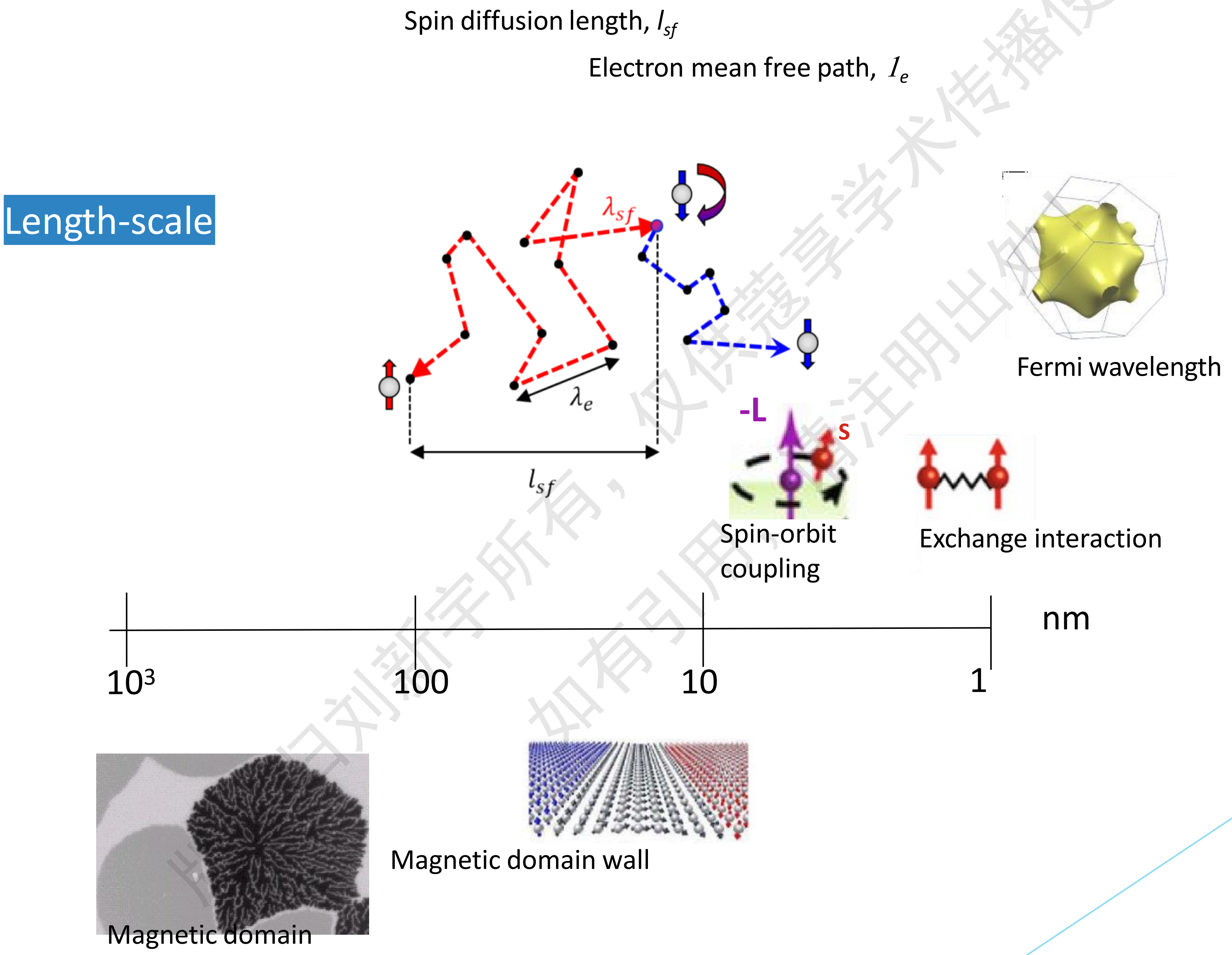

Length- and energy-scales

Time- and energy scales